Linking the Collisional History of the Main Asteroid Belt to its Dynamical Excitation and Depletion

William F. Bottke, Jr.[1]

Daniel D. Durda[1]

David Nesvorný[1]

Robert Jedicke[2]

Alessandro Morbidelli[3]

David Vokrouhlický[4]

Harold F. Levison[1]

[1]Southwest Research Institute, 1050 Walnut St, Suite 400, Boulder, CO 80302
[2]Institute for Astronomy, University of Hawaii, Honolulu, Hawaii 96822-1897
[3]Obs. de la Côte d'Azur, B.P. 4229, 06034 Nice Cedex 4, France
[4]Institute of Astronomy, Charles University, V Holešovičkách 2, 180 00 Prague 8, Czech Republic

Prepared for *Icarus*

May 27, 2005

77 manuscript pages
1 table
16 figures (2 in color)

Running Head:
Collisional and Dynamical Evolution of Main Asteroid Belt
Editorial Correspondence and Proofs:

William F. Bottke, Jr.
Department of Space Studies
Southwest Research Institute
1050 Walnut St, Suite 400
Boulder, CO 80302

Tel: (303) 546-6066
Fax: (303) 546-9687
E-mail: bottke@boulder.swri.edu

ABSTRACT

The main belt is believed to have originally contained an Earth mass or more of material, enough to allow the asteroids to accrete on relatively short timescales (e.g., Weidenschilling 1977). The present-day main belt, however, only contains $\sim 5 \times 10^{-4} M_\oplus$. Numerical simulations suggest that this mass loss can be explained by the dynamical depletion of main belt material via gravitational perturbations from planetary embryos and a newly-formed Jupiter. To explore this scenario, we combined dynamical results from Petit *et al.* (2001) with a collisional evolution code capable of tracking how the main belt undergoes comminution and dynamical depletion over 4.6 Gy (Bottke *et al.* 2005). Our results were constrained by the main belt's size-frequency distribution, the number of asteroid families produced by disruption events from diameter $D > 100$ km parent bodies over the last 3-4 Gy, the presence of a single large impact crater on Vesta's intact basaltic crust, and the relatively constant lunar and terrestrial impactor flux over the last 3 Gy. We used our model to set limits on the initial size of the main belt as well as Jupiter's formation time.

We find the most likely formation time for Jupiter was 3.3 ± 2.6 My after the onset of fragmentation in the main belt. These results are consistent with the estimated mean disk lifetime of 3 My predicted by Haisch *et al.* (2001). The post-accretion main belt population, in the form of diameter $D \lesssim 1000$ km planetesimals, was likely to have been 160 ± 40 times the current main belt's mass. This corresponds to 0.06-$0.1 M_\oplus$, only a small fraction of the total mass thought to have existed in the main belt zone during planet formation. The remaining mass was most likely taken up by planetary embryos formed in the same region. Our results suggest that numerous $D > 200$ km planetesimals disrupted early in solar system history, but only a small fraction of their fragments survived the dynamical depletion event described above. We believe this may explain the limited presence of iron-rich M-type, olivine- rich A-type, and non-Vesta V-type asteroids in the main belt today. The collisional lifetimes determined for main belt asteroids agree with the cosmic ray exposure ages of stony meteorites and are consistent with the limited collisional evolution detected among large Koronis family members.

Using the same model, we investigated the near-Earth object (NEO) population. We show the shape of the NEO size distribution is a reflection of the main belt population, with main belt asteroids driven to resonances by Yarkovsky thermal forces. We used our model of the NEO population over the last 3 Gy, which is consistent with the current population determined by telescopic and satellite data, to explore whether the majority of small craters ($D < 0.1$-1 km) formed on Mercury, the Moon, and Mars were produced by primary impacts or by secondary impacts generated by ejecta from large craters. Our results suggest that most small craters formed on these worlds were a byproduct of secondary rather than primary impacts.

1. Introduction

The collisional and dynamical history of the main belt is strongly linked with the growth and evolution of the planets, with the events occurring during this primeval era recorded in the orbits, sizes, and compositional distributions of the asteroids and in the hand sample of meteorites. Like archaeologists working to translate stone carvings left behind by ancient civilizations, the collisional and dynamical clues left behind in or derived from the main belt, once properly interpreted, can be used to read the history of the inner solar system. From a practical standpoint, this means we not only have to understand how asteroids have been scarred and fragmented over time by hypervelocity impacts but also how gravitational perturbations from planets, planetary embryos, and the solar nebula have affected the orbital distribution of the survivors.

The foundation for the work presented in this paper is Bottke *et al.* (2005) (hereafter B05), who used numerical simulations to track how the initial main belt size frequency distribution was affected over time by comminution and fragmentation. The constraints used in their modeling work, namely the wavy-shaped main belt size-frequency distribution, the quantity of asteroid families produced by the disruption of $D > 100$ km parent bodies over the last 3-4 Gy, the cratered surface of asteroid (4) Vesta, and the relatively constant crater production rate of the Earth and Moon over the last 3 Gy, were wide ranging enough for them to estimate the shape of the initial main belt size frequency distribution as well as the asteroid disruption scaling law Q_D^*, a critical function needed in all codes that include fragmentation between rocky planetesimals. In contrast to previous efforts (e.g., Durda *et al.* 1998), B05 demonstrated that the Q_D^* scaling laws most likely to produce current main belt conditions were similar to those generated by recent smoothed particle hydrodynamic (SPH) simulations (e.g., Benz and Asphaug 1999). They also showed there was a limit to the degree of main belt comminution that could have taken place over solar system history; too much or too little would produce model size distributions discordant with observations. In fact, they suggested that if the current main belt were run backwards in time, it would need the equivalent of roughly 7.5-9.5 Gy of "reverse comminution" to return to its initial state, a time interval roughly twice as long as the age of the solar system (4.6 Gy).

To explain this puzzling result, B05 argued the extra comminution had to come from a collisional phase occurring early in solar system history ($\sim$ 3.9-4.5 Ga) when the primordial main belt held significantly more diameter $D < 1000$ km bodies than it contains today. The extra material in this population would have been removed by dynamical rather than collisional processes. What B05 left out of their simulations, however, was a way to account for the excitation and elimination of main belt material by dynamical processes. They did this for two reasons. The first was that including dynamical processes into their simulations would have increased their number of unknown parameters, enough that obtaining unique solutions for Q_D^* and the initial shape of the main belt size distribution would have been impossible. The second is that they wanted to avoid locking themselves into a dynamical evolution scenario that would likely become obsolete as planet formation models increased in sophistication (e.g., next generation models will likely include the effects of dynamical friction between planetary embryos and planetesimals,

gas drag on planetesimals, planetary migration, and the nature and effects of the so-called Late Heavy Bombardment; Hartmann *et al.* 2000; Gomes *et al.* 2005; see Sec. 2.2.4). Instead, B05 used a more approximate approach that retained the essential aspects of the problem but made simplifying assumptions (e.g., they assumed that most main belt comminution occurred when collisional probabilities and impact velocities were comparable to current values; a massive population experiencing comminution over a short interval is mathematically equivalent to a low mass population undergoing comminution over an extended interval). Thus, rather than modeling the collisional and dynamical history of the main belt over 4.6 Gy, B05 instead tracked how a population comparable in mass to the current main belt would evolve over timescales longer than the age of the solar system, with the extra simulation time compensating for a (putative) early phase of comminution occurring when the main belt was both excited and massive.

Using insights provided by B05, we are now ready to try a more ambitious model that directly accounts for both collisional and dynamical processes over the last 4.6 Gy. Here we combine results from the best available dynamical model of early main belt evolution (Petit *et al.* 2001) with the collision code and best fit results of B05. As we show below, the results from this hybrid code can be used to estimate the initial mass of the $D < 1000$ km population in the primordial main belt, constrain the formation timescale of Jupiter, and produce a more refined understanding of the nature of the dynamical depletion event that scattered bodies out of main belt population early in solar system history. Thus, we argue the main belt provides us with critical clues that can help us probe the nature of planet formation events in the inner solar system.

To verify our results, we made numerous comparisons between our model's predictions and the available constraints, with our results showing an excellent match between the two. These predictions include estimates of: (i) the post-accretion size distribution found among main belt planetesimals, (ii) the disruption scaling law controlling asteroid breakup events, (iii) the collisional lifetime of main belt asteroids, and (iv) the main belt and NEO population size distributions over a size range stretching from cm- to Ceres-sized objects over the last 4.6 Gy. Using our NEO population model, we also investigated the nature of small craters on the terrestrial planets and whether they were formed by primary impacts or by secondary impacts produced by ejecta from large craters. For those wishing to see a detailed summary of our results before reading the paper, please turn to our Conclusions in Sec. 7.

Here we provide a brief outline for this paper. In Sec. 2, we discuss the current state of the art in main belt dynamical evolution models, and closely examine the results described by Petit *et al.* (2001), whose model does the best job thus far of explaining the available dynamical constraints. In Sec. 3, we show how the dynamical excitation and depletion of the main belt, as well as the effects of Yarkovsky thermal forces, are included in our model. We also review our principal model constraints. In Sec. 4, we discuss several trial runs of our model while also presenting our large-scale production runs. In Sec. 5, we discuss the numerous implications of our results, which extend into many issues of main belt and NEO evolution. Finally, in Sec. 6, we present our conclusions.

One additional comment should be made here. In B05, we reviewed the history of main belt collisional evolution models. Since that time, an additional model has been submitted (O'Brien and Greenberg 2005) and another published (Cheng 2004). Between the two, the O'Brien and Greenberg (2005) model is more similar to one presented here, though there are several distinct differences in the choices made for initial conditions, model components and constraints, methods, and in the treatment of the dynamical evolution of the primordial main belt. The most important difference between these two papers and ours, however, is that our results were constrained by the observed distribution of asteroid families formed over the last 3.5 Gy whose parent bodies had diameter $D > 100$ km (see Sec. 3.4 and B05). We were literally driven to the results described below by these data, which allowed us to eliminate many unrealistic input parameters. We believe any future models of main belt evolution will need to be similarly tested in order to obtain unique solutions.

2.   Models for the Dynamical Evolution and Depletion of the Main Belt

2.1.   Previous Work

To determine the nature of the dynamical excitation and depletion event that affected the main belt, we first need to understand the dynamical constraints provided by main belt asteroids (a recent review of this issue can be found in Petit *et al.* 2001; 2002). One powerful constraint concerns the putative depletion of material in the main belt zone. While the main belt only contains $\sim 5 \times 10^{-4} M_\oplus$ of material today, it may have once held an $M_\oplus$ or more of material (Weidenschilling 1977; Lissauer 1987). The fate of this missing mass is uncertain, but numerical models suggest most of this mass was ejected from the main belt zone shortly after the end of the accretion phase (e.g., see Petit *et al.* 2002 for a review).

A second constraint comes from the current dynamical excitation of the largest main belt bodies. The 682 asteroids with diameter $D > 50$ km have eccentricities e and inclinations i spread between 0-0.3 and 0°-30°, respectively. These values are large enough that collisions produce fragmentation rather than accretion (Farinella and Davis 1992; Bottke *et al.* 1994a; Petit *et al.* 2001). Because this could not have been true when the asteroids were accreting, some dynamical mechanism must have modified their orbits from low (e, i) values to the excited and widely-distributed values seen today.

Finally, the distribution and (partial) radial mixing of taxonomic classes found among the largest asteroids ($D > 50$ km) provides a third dynamical constraint. Gradie and Tedesco (1982) showed that large S-type asteroids dominate the inner belt (semimajor axis a between 2.1-2.5 AU) while C-types dominate the central belt ($2.5 < a < 3.2$ AU and D-/P-types dominating the outer main belt ($a > 3.2$ AU). The boundaries between these groups, however, are not sharp, with some C and D asteroids found in the inner main belt and some S-types found in the outer main belt. It is unlikely that thermal evolution alone produced this configuration (Grimm and

McSween 1993; see review by McSween *et al.* 2002). Instead, it is plausible that some process (or processes) partially mixed the taxonomic types after accretion. Note that we exclude from our discussion the semimajor axis distribution trends for $D < 50$ km asteroids (Mothé- Diniz *et al.* 2003), partly because many of them are fragments produced by large-scale disruption events (B05) but also because $D \lesssim$ 20-30 km asteroids are susceptible to significant semimajor axis drift via the Yarkovsky effect (e.g., Farinella and Vokrouhlický 1999; Bottke *et al.* 2002a).

To explain these features, several research groups have investigated dynamical mechanisms capable of exciting asteroidal eccentricities/inclinations and potentially removing primordial asteroids from the main belt. Some of the earliest work on this issue was described by Safronov (1969), who suggested that Jupiter-scattered protoplanets during the planet formation epoch could have interacted with and dispersed numerous primordial asteroids. Ideally, this scenario could explain the termination of accretion in the main belt, the onset of fragmentation, why main belt asteroids are in a dynamically excited state and why the largest asteroids show signs of limited radial mixing. Numerical results, however, indicate that Jupiter-scattered protoplanets would produce an excitation gradient in the main belt, with bodies between $2 < a < 3$ AU far less excited than those with $a > 3$ AU (Petit *et al.* 1999; see also Davis *et al.* 1979; Ip 1987; Wetherill 1989). Because this excitation gradient is not observed, it appears unlikely the primordial main belt lost a significant amount of mass in this manner.

Another potential way to dynamically excite and depopulate the main belt is by sweeping secular resonances. They can be launched by a uniformly-decaying solar nebula (Ward 1979; 1981; Heppenheimer 1980; Ida and Lin 1996; Liou and Malhotra 1997; Franklin and Lecar 2000; Nagasawa *et al.* 2000), a non-uniformly decaying nebula (e.g., Nagasawa *et al.* 2000; see Petit *et al.* 2002 for a short review of various nebular depletion mechanisms), or by migrating planets (Gomes 1997; Kortenkamp and Wetherill 2000; Kortenkamp *et al.* 2001; Levison *et al.* 2001). For the nebular case, interactions between newly-formed giant planets and a massive solar nebula produce secular resonances fixed to particular orbital positions. As the solar nebula disperses, these secular resonances gradually move to new orbital positions and sweep through regions that may contain planetesimals. For migrating planets, secular and mean motion resonances can change positions if planets like Jupiter or Saturn take on new a, e, and/or i values. Objects encountering these resonances can have their own (e, i) values modified. Thus, in an idealized scenario, sweeping resonances would scatter most of the bodies out of the primordial main belt, leaving behind a small remainder with the main belt's observed range of (e, i) values.

Current numerical modeling work, however, indicates these scenarios cannot yet satisfy the main belt constraints described above. Nagasawa *et al.* (2000) shows that sweeping secular resonances acting on test bodies with circular, low-i orbits can be depleted from the main belt, but at the cost of leaving the survivors with a narrow ranges of i values; such values are not observed. They also tend to remove too much of the main belt's mass from the wrong places (Levison *et al.* 2001). In addition, sweeping secular resonances do not affect semimajor axis values and therefore cannot explain the mixture of taxonomic types seen among the largest asteroids. Models where

Jupiter and Saturn form and migrate very early in solar system history also appear to prevent the formation of large asteroids like Ceres (Kortenkamp and Wetherill 2000; Kortenkamp *et al.* 2001). With this said, it is possible that secular resonances, driven by the migration of the Jovian planets, did sweep across a main belt that was already dynamically excited, but perhaps not until the Late Heavy Bombardment epoch ~ 3.9 Ga (Levison *et al.* 2001; Gomes *et al.* 2005; see also Sec. 2.2.4).

Finally, some have investigated the idea that planetary embryos grown inside the main belt not only produced its dynamically-excited state but also contributed to its dynamical depletion. This scenario, which was originally developed by Wetherill (1992) and further pursued by several other research groups (Chambers and Wetherill 1998; Chambers and Wetherill 2001; Petit *et al.* 2001), arguably provides the best match *at present* with main belt dynamical constraints among existing models (see Petit *et al.* 2001; 2002 for details). For this reason, we describe this scenario in greater detail below.

2.2. Dynamical Excitation and Depletion of the Main Belt by Planetary Embryos

The dynamical history of the main belt via planetary embryo evolution can be divided into three somewhat broadly-defined phases that we describe below.

2.2.1. Phase 1: Dynamical Excitation of the Primordial Main Belt

According to the core-accretion model, runaway growth among planetesimals should produce Moon- to Mars-size planetesimals throughout the inner solar system (e.g., Safronov 1969; Greenberg *et al.* 1979; Wetherill and Stewart 1989; Weidenschilling *et al.* 1997; Kokubo and Ida 2002). The timescale of embryo growth throughout the inner solar system is unknown, though it is believed Moon to Mars-sized objects could have grown in less, perhaps much less, than a few My. This would explain how Jupiter accreted a several $M_{\oplus}$ core capable of amassing its atmosphere before the solar nebula was eliminated (Pollack *et al.* 1996; Wuchterl *et al.* 2000; Inaba *et al.* 2003; Podolak 2003; Hubickyj *et al.* 2003; Alibert *et al.* 2004). The estimated lifetime of protoplanetary disks, according to an analysis of dust emission around objects in various star clusters, is 1-10 My, where approximately half of the stars lose their disks in ≤ 3 My (Haisch *et al.* 2001).

Models describing the evolution of planetary embryos and planetesimals in the inner solar system have been described by several groups (Agnor *et al.* 1998; Chambers and Wetherill 1998; 2001; Chambers and Cassen 2002). Here we focus on the results provided by Petit *et al.* (2001), who investigated the dynamical excitation of the asteroid belt by both planetary embryos and Jupiter (see also Morbidelli *et al.* 2000; 2001). Petit *et al.* first tracked the evolution of 56 embryos started on circular, slightly inclined orbits (0.1°) between 0.5 and 4 AU using the MERCURY integration package (Chambers and Migliorini 1997). The total mass of these embryos was $5M_{\oplus}$, consistent with the expected primordial mass of solids in that region (Weidenschilling 1977). The

masses of the individual embryos were increased from the inner (1/60 Earth mass) to the outer edge (1/3 Earth mass) of the disk according to $\propto a^3 \sigma^{-3/2}$, where σ is the surface density of the protoplanetary disk. In this formative stage, the embryos were separated by a fixed number of mutual Hill radii. The increase in mass was chosen such that the surface density σ was proportional to a^{-1}.

Fig. 1 shows the dynamical evolution of the embryos prior to the formation of Jupiter, which was set somewhat arbitrarily to 10 My. The embryos are represented by the large grey particles. The approximate region represented by the current main belt in (a, e, i) space is shown by the solid black lines. We see that the embryos gravitationally perturb one another enough over 10 My to initiate some mergers and moderately excite themselves (e values reach ~ 0.4; i values reach $\sim 30°$. The innermost embryos are the dynamically "hottest", while those beyond 4 AU remain relatively "cold".

EDITOR: PLACE FIGURE 1 HERE.

Using this embryo evolution dataset, Petit *et al.* (2001) created several simulations where the recorded positions and masses of the embryos were used to gravitationally perturb test bodies initially placed on circular, zero-i orbits. Fig. 1 also shows the evolution of 100 test bodies started with semimajor axes equally spaced between 2 and 3.5 AU. These test bodies are designed to represent asteroids in the primordial main belt that failed to accrete with various planetary embryos during runaway growth. The dynamical evolution of the test bodies was tracked using the numerical integrator SWIFT-RMVS3 (Levison and Duncan 1994), with perturbations of the planetary embryos included using techniques described by Petit *et al.* (1999). Snapshots of their (a, e, i) values at 0, 3, and 10 My are shown in Fig. 1 as small black dots. By 10 My, the e values of some test bodies reach ~ 0.6, while their i values extend up to $\sim 40°$. The consequences of this, as we will describe below, are to increase collision velocities enough to initiate fragmentation during impacts.

2.2.2. *Phase 2: Dynamical Depletion of the Main Belt*

At some time during Phase 1, runaway growth produced a several $M_\oplus$ core near Jupiter's current location (Wuchterl *et al.* 2000; Inaba *et al.* 2003). Modeling results suggest this planetary embryo was massive enough to accrete gas from the solar nebula (Pollack *et al.* 1996; Podolak 2003; Hubickyj *et al.* 2003; Alibert *et al.* 2004). Because Jupiter formed before the gaseous component of the disk was lost, its formation age was approximately 1-10 My after the formation of the first solids (Haisch *et al.* 2001).

The introduction of Jupiter (and Saturn) into the solar system, which we mark as the beginning of Phase 2, had a dramatic effect on the dynamical structure of the primordial main

belt. To simulate this, Petit *et al.* (2001) introduced Jupiter and Saturn into the evolving system of embryos at 10 My, assuming they had their present-day masses and (a, e, i) values. Fig. 2 shows how these bodies affect planetary embryos in the main belt. Close encounters with Jupiter quickly throw several embryos out of the inner solar system. Gravitational perturbations from Jupiter and Saturn also introduce a secular oscillation into the embryos' eccentricities. When combined with the mutual gravitational perturbations from the embryos and the addition of Jupiter/Saturn's mean motion/secular resonance structure, the net effect is to radically increase the dynamical temperature of the system (i.e., the embryos obtain larger e, i values). In this simulation, embryos push one another out of the main belt, explaining why none are seen there today (e.g., Chambers and Wetherill 2001).

EDITOR: PLACE FIGURE 2 HERE.

The embryos continued to merge until they formed a system similar to that of our terrestrial planets. Fig. 3 shows all of the unstable embryos have been eliminated by $t = 100$ My. The planets remaining have a mass of $1.3 M_{\oplus}$ ($a = 0.68$ AU, $e = 0.15$, and $i = 5°$) and $0.48 M_{\oplus}$ ($a = 1.5$ AU, $e = 0.03$, and $i = 23°$).

This simulation illustrates the success and failures of the current generation of late-stage planet formation models. We can see that it is possible to generate terrestrial planet systems reminiscent of our Solar System, but the planets are dynamically hotter than the Earth and Venus. The timescales needed to complete the terrestrial planets are also longer than suggested by the Moon- forming impact on Earth ($\sim$ 25-30 My after the formation of the solar system), which likely marked the end of significant accretion on Earth (see review by Canup 2004). We suspect that to create systems closer to our own, next-generation codes will need to account for important physical processes such as dynamical friction between the large and small bodies, gas drag, gravitational interactions with the gas component of the disk, and fragmentation. Despite these limitations, however, the terrestrial planets produced in Petit *et al.* (2001) do not cross into the main belt zone, making them comparable enough to our own system that we can use them to probe the evolution of the primordial main belt.

EDITOR: PLACE FIGURE 3 HERE.

To determine what happened to the main belt after the formation of Jupiter, Petit *et al.* (2001) inserted 100 test bodies on circular orbits between 1.0-2.0 AU (simulation A4) and 1000 test bodies between 2.0-2.8 AU (simulation A3) into the embryo/Jupiter/Saturn system described above. The initial conditions are shown in Fig. 2. The test bodies were tracked for 100 My, with their orbits modified by the combined perturbations of the embryos and Jupiter/Saturn. Details of the integration can be found in Petit *et al.* (2001). We show the results as a series of snapshots in Figs. 2 and 3. The test bodies are shown as small black dots. The objects left behind and/or

dynamically trapped on stable orbits in the main belt have black/gray squares around them (gray was used for the 15 My timestep so the square could be seen against the black dot background). Note that several black square objects spend time outside the main belt zone before perturbations from planetary embryos capture them in the main belt once again.

The simulations show that the eccentricities and inclinations of test bodies from both populations become highly excited over just a few My, with most objects eliminated by striking the Sun or being thrown out of the inner solar system via a close encounter with Jupiter. For the 1000 bodies started between 2.0-2.8 AU, five objects survived to reach the asteroid belt: one in the inner belt (2.0-2.5 AU), three in the central belt (2.5-3.28 AU), and one in the outer belt (> 3.28 AU). All the survivors started with a between 2.5-2.8 AU. These results imply that the main belt may have dynamically lost $\gtrsim 99\%$ of its primordial material via dynamical excitation. We will refer to this in this paper as the "dynamical depletion event" (DDE).

For the 100 bodies started between 1.0-2.0 AU, most reach extremely high e (0.6-1.0) and i values ($> 40°$). If collisions were included here, these objects would be able to collide with the main belt survivors (black squares) at high impact velocities over a time span of tens to hundreds of My (see Sec. 3.2).

At 100 My, nearly all the test bodies are gone; only 9 objects remain from the 1000 test body set started between 2.0-2.8 AU (5 in the main belt), while 3 remain from the 100 test body set started between 1.0-2.0 AU. To study their evolution, Morbidelli *et al.* (2001) created 200 clones of these particles and continued their integrations for an additional 400 My. They found the high inclination population had a median dynamical lifetime of 60 My, roughly a factor of 10 longer than typical near-Earth objects (e.g., Gladman *et al.* l997; Bottke *et al.* 2000; Bottke *et al.* 2002b).

We combined the results of these simulations to estimate the decay rate of excited planetesimals in the inner solar system. Runs between 0-10 My result in virtually no loss of material. To get the decay rate for test bodies between 10-100 My, we multiplied the results of the 100 test body run started between 1.0-2.0 AU by a factor of 10 in order to equate them with the 1000 test body runs started between 2.0-2.8 AU runs. These results were then merged with the 100-500 My runs described above. Fig. 4 shows that the excited planetesimal population drops steeply once Jupiter enters the system at 10 My. By ~ 15 My, half of the population has been eliminated. Only 10% are left at 50 My, while 2% are left at 100 My. Finally, at ~ 400 My, the last excited (cloned) test body was eliminated, leaving behind a population of main belt survivors comprising 0.5% of the initial population.

EDITOR: PLACE FIGURE 4 HERE.

2.2.3. Phase 3: Collisional Evolution in a Depleted Main Belt

Phase 3 begins when the population described in Phase 2 has been depleted of material. Here gravitational interactions between asteroids and embryos have not only left the main belt in a dynamical state comparable to the current population, but the semimajor axis distances traversed by the survivors is of the same order as the S- and C-type mixing observed among large main belt asteroids (Petit *et al.* 2001). These interactions have also scattered any asteroid families produced in Phases 1-2. This leaves the Phase 3 main belt as a *tabula rasa* for new family formation.

The loss of main belt material in Phase 3 is produced both by collisions and the Yarkovsky effect, which drives $D \lesssim 30$ km asteroids into mean motion and secular resonances that can pump up their eccentricities to planet-crossing values (Farinella and Vokrouhlický 1999; Bottke *et al.* 2000; 2001; 2002a,b). The relatively constant loss of material during this phase is believed to explain the steady state population of the near-Earth object population as well as the nearly-constant crater production rates observed on the lunar maria over the last 3 Gyr (within a factor of 2 or so) (Grieve and Shoemaker 1994; Shoemaker and Shoemaker 1996; McEwen *et al.* 1997; Shoemaker 1998; Morbidelli and Vokrouhlický 2003; B05).

2.2.4. Caveats and Model Limitations

The principal unknown quantity to understanding main belt evolution during Phase 3 is the nature of the Late Heavy Bombardment (LHB) that occurred ~ 3.8-4.0 Ga (e.g., Tera *et al.* 1974; Hartmann *et al.* 1981; 2000). It was during the LHB that the lunar basins with known ages were formed (e.g., the diameter $D = 860$ km Nectaris basin formed 3.90-3.92 Ga; the $D = 1200$ km Imbrium basin formed 3.85 Ga; the $D = 930$ km Orientale basin formed 3.82 Ga; Wilhelms *et al.* 1987). Some argue the LHB was produced as part of the tail end of accretion (e.g., Hartung 1974; Hartmann 1975; Grinspoon 1989; Neukum and Ivanov 1994) while others say it was a terminal cataclysm produced by a "spike" in the impact rate at ~ 3.8 Ga (e.g., Ryder *et al.* 2000).

Although the LHB's origin and length are unknown, recent numerical studies have suggested an intriguing possibility: the LHB may have been caused by a sudden dynamical depletion of small bodies in the primordial outer solar system ~ 3.9 Ga (e.g., Levison *et al.* 2001). For example, Gomes *et al.* (2005) examined the migration of the 4 outer planets interacting with a planetesimal disk of 10-50$M_\oplus$ truncated at 30 AU. In their simulations, all the planets were initially set on nearly circular, co-planar orbits, but were given a more compact configuration (within 15 AU), presumably to allow Uranus and Neptune to accrete over short timescales (Thommes *et al.* 1999; 2002; Levison and Stewart 2001). Slow planetary migration was induced by bodies leaking out of the disk and encountering Neptune. These interactions slowly but steadily stretched the system of planets. Eventually, after a delay of several hundred My, Jupiter and Saturn crossed their 1:2 mean motion resonance, which in turn caused their e and i-values to jump from near zero to their current values. At the same time, Uranus and Neptune were scattered outward, allowing them to

penetrate the disk, migrate through it, and send numerous comets toward the inner solar system.

With Jupiter and Saturn shifting to new orbits, inner solar system resonances like the ν_6 and ν_{16} secular resonances would have also been forced to move to new locations. Numerical simulations suggest they may have swept across the main belt region, which would have ejected numerous asteroids from that stable zone. Thus, if this scenario is realistic, the LHB may be a combination of cometary bodies scattered by Uranus/Neptune and asteroids ejected from the main belt reservoirs.

A Gomes *et al.* (2005) type LHB would have several important consequences for the work presented here. The first is that projectiles from the LHB could have disrupted main belt asteroids. The second is that the migration of the Jovian planets may have caused numerous asteroids to have been dispersed, trapped, excited, or even ejected from the main belt zone. Finally, if the main belt did lose a significant fraction of its mass 3.9 Ga, it would imply that the population surviving the first DDE in Phase 2 was perhaps ~ 10 times larger than the current population for 3.9-4.5 Ga. This extra material would produce an elevated interval of comminution lasting ~ 600 My.

Because B05 showed the main belt can only sustain a limited degree of collisional evolution, it is unclear to us whether the model presented here can accommodate the large number of "bonus" collisions produced in a Gomes *et al.* (2005) scenario. In fact, to match main belt constraints, we would likely need to decrease comminution during Phases 1-2 in some fashion. Interestingly, more advanced planet formation models could work in this direction. For example, the inclusion of gas in the disk might help damp the (e, i) values of planetesimals excited by gravitational interactions with embryos. In turn, dynamical friction between planetary embryos and damped planetesimals could keep the dynamical temperature of the embryos lower than described in Petit *et al.* (2001). Gas in the disk might also induce migration among the embryos, which in turn could lead to more reasonable terrestrial planet formation timescales (McNeil *et al.* 2005).

Although these issues are thought provoking, we consider it premature to include them into our model at this time. The Gomes *et al.* (2005) scenario, while interesting, is currently in its infancy, while no one knows precisely how the inclusion of gas and dynamical friction into planet formation models will affect the main belt. Nevertheless, we believe the history of the main belt (and the solar system) is intimately linked to our understanding of planet formation and the LHB, such that we may need to revisit this topic in the near future.

3. Modeling the Collisional Evolution of the Main Belt Size Distribution

To model the evolution of the main belt as completely as possible, we integrated the dynamical results described in Sec. 2.2 (Petit *et al.* 2001) with the collisional evolution code CoEM-ST (B05). Our modified code, called CoDDEM (for collisional and dynamical depletion model), is described below in two parts. In the first part, we briefly describe our nominal model (CoEM-ST). In the second part, we describe the modifications needed to allow our model to account for the dynamical

ejection of $\gtrsim 99\%$ of the main belt's primordial mass.

3.1. Nominal collisional model

Our nominal model is called CoEM-ST, which stands for collisional evolution model, stochastic breakup version; a full description of this code can be found in B05. It takes as input an initial size-frequency distribution where the population (N) has been binned between 0.001 km $< D <$ 1000 km in logarithmic intervals $d \log D = 0.1$. The particles in the bins are assumed to be spherical and are set to a bulk density of 2.7 g cm^{-3}; modest changes to this value do not affect our results. CoEM-ST then computes the time rate of change per unit volume of space over a size range between diameter D and $D + dD$ (Dohnanyi 1969; Williams and Wetherill 1994):

$$\frac{\partial N}{\partial t}(D, t) = -I_{\text{DISRUPT}} + I_{\text{FRAG}} - I_{\text{DYN}}. \tag{1}$$

I_{DISRUPT} is the net number of bodies that leave between D and $D + dD$ per unit time from catastrophic disruption. I_{FRAG} is the number of bodies entering the size bin per unit time that were produced via the fragmentation of larger bodies. Note that main belt cratering events are not included in our model because they produce significantly less ejecta over time than catastrophic collisions (e.g., Dohnanyi 1969; Williams and Wetherill 1994). I_{DYN} is the number of bodies lost from the size bin via dynamical processes. Note that I_{DYN} was not used in CoEM-ST (B05) but it will be here.

We define I_{DISRUPT} as:

$$I_{\text{DISRUPT}} = \frac{N}{\tau} \tag{2}$$

where τ is the collisional lifetime of a body between D and $D + dD$. Assuming a projectile of diameter D_{disrupt} can barely disrupt a target asteroid of diameter D_{T} (see below), the lifetime of the target body (τ) becomes:

$$\frac{1}{\tau} = \frac{P_i}{4} \int_{D_{\text{disrupt}}}^{D_{\text{T}}} (D_{\text{T}} + D')^2 N(D', t) \mathrm{d}D' \tag{3}$$

where P_i is the "intrinsic collision probability", the probability that a single member of the impacting population will hit a unit area of the target body in a unit of time (Öpik 1951; Wetherill 1967; Greenberg 1982; Farinella and Davis 1992; Bottke and Greenberg 1993).[1] The effects of gravitational focussing are neglected here.

---

[1] An asteroid's cross-section is usually defined as $(\pi/4)D_{\text{T}}^2$, but here the π value is included in P_i.

The projectile capable of disrupting D_{T} is:

$$D_{\mathrm{disrupt}} = (2Q_{\mathrm{D}}^*/V_{\mathrm{imp}}^2)^{1/3} D_{\mathrm{T}} \tag{4}$$

The impact velocity is V_{imp}, while Q_{D}^* is the critical impact specific energy, or the energy per unit target mass needed to disrupt the target and send 50% of its mass away at escape velocity. In this paper, we examine the Q_{D}^* functions derived by B05 that provide excellent fits to the main belt's constraints. They are defined as a rotated and translated hyperbola in $\log Q_{\mathrm{D}}^*$ and $\log D$ space:

$$E\Delta x^2 + F\Delta x\Delta y + G\Delta y^2 + H = 0 \tag{5}$$

where E, F, G, and H are constants, $\Delta x = x - x_0$, $x = \log D$ (km), $\Delta y = y - y_0$, $y = \log Q_{\mathrm{D}}^*$ (erg g^{-1}), $x_0 = -0.753$ and $y_0 = 2.10$. (Fig. 5). Note that our Q_{D}^* function passes through the normalization point $Q_{\mathrm{D}}^* = 1.5 \times 10^7$ erg g^{-1} and $D = 8$ cm, a value determined using laboratory impact experiments (e.g., Durda *et al.* 1998).

In this paper, we use many of the best-fit Q_{D}^* functions identified by B05 (Fig. 5). More specifically, using the B05 numbering scheme, we test Q_{D}^* functions #7-14. Our results indicate that Q_{D}^* functions outside the #7-14 range are unlikely to produce results superior to those discussed below. The Eq. (5) parameters for #7 are $E = 0.895, F = -0.782, G = -0.455$, and $H = -0.276$ and those for #14 are $E = 0.864, F = -0.904, G = -0.499$, and $H = -0.305$. For reference, the red curve on Fig. 5, labeled as #13, is the Q_{D}^* function predicted by the hydrocode modeling results of Benz and Asphaug (1999).

<div align="center">EDITOR: PLACE FIGURE 5 HERE.</div>

Once D_{disrupt} is known, the number of objects with $D_{\mathrm{disrupt}} < D < D_{\mathrm{T}}$ is computed from the input size distribution. If D_{disrupt} is smaller than the smallest bin available in CoEM-ST, the number of projectiles is estimated by extrapolating the shape of the small end of the size distribution to the required value of D_{disrupt}. With all components in hand, CoEM-ST computes the collisional lifetime τ for each size bin. The timestep for the evolution model is automatically set to be 10 times smaller than the minimum τ value.

To remove disrupted bodies from our size-frequency distribution, CoEM-ST treated breakup events as random events, with integer numbers of particles removed (or not removed) from a size bin within a timestep according to Poisson statistics (Press *et al.* 1989). Because this procedure is not deterministic, different seeds for the random number generator may produce different outcomes. Therefore, to get a quantitative measure of how good a given set of input parameters reproduces observations, we need to perform numerous CoEM-ST trial cases.

To determine I_{FRAG}, and to keep things as simple as possible given our unknowns in this area, B05 assumed the fragment size distribution (FSD) produced by each catastrophic disruption event was similar to those observed in asteroid families like Themis (super-catastrophic) or Flora (barely-catastrophic) (Tanga *et al.* 1999; see B05 for details). Here we assume the differential FSDs have the form $dN = BD^p dD$, with dN the differential number of fragments between D and $D + dD$, B a constant, and p the power law index (e.g., Colwell 1993). Themis-like FSDs were developed for $D > 150$ km disruption events. We assumed the largest remnant was 50% the diameter of the parent body. The differential power law index between the largest remnant and fragments 1/60th the diameter of the parent body was -3.5. Fragments smaller than 1/60th the diameter of the parent body follow a power law index of -1.5. Flora-style FSDs were developed for breakups among $D < 150$ km bodies. Here the diameter of the largest remnant is set to 80% the diameter of the parent body. We gave these FSDs power law indices, from the large end to the small end, of -2.3, -4.0, and -2.0, with transition points at 1/3 and 1/40 the diameter of the parent body. Note that in both cases, we assume that some material is located below the smallest size used by CoDDEM ($D = 0.001$ km) in the form of small fragments or regolith. Accordingly, mass is roughly but not explicitly conserved. Additional detail on these values, as well as their effect of main belt evolution, can be found in B05.

Finally, CoDDEM does not track how putative effects like embryo-embryo collisions or tidal disruption between embryos and planetesimals could change the main belt's size frequency distribution (e.g., Agnor and Asphaug 2004; Asphaug *et al.* 2005). We leave these interesting issues to future work. At present, we can only say that, based on spectroscopic and mineralogical studies of asteroids and meteorites, it seems unlikely that fragments from Moon- to Mars-sized planetary embryos make up a significant fraction of the current main belt (e.g., Gradie and Tedesco 1982; Keil 2002; Scott 2002; H. McSween, personal communication).

3.2. Including dynamical depletion into the nominal collisional model

3.2.1. Methodology

To account for dynamical depletion in CoEM-ST, we start with the assumption that asteroid collisions occur infrequently enough during the post-accretion phase that they do not significantly damp the (e, i) values of asteroids excited by any dynamical mechanism. This means our collisional and dynamical evolution results are decoupled, such that we can simulate the dynamics first, characterizing those results using parameters like P_i and V_{imp}, and then include them in our collisional model. We justify this using results from B05, who showed that the main belt only experienced a limited degree of comminution throughout solar system history.

Using this idea, we, like B05, divide our initial main belt population into two components, a small component of main belt asteroids that we know will survive the DDE described in Phase 2 (N_{rem}, where "rem" stands for remnant population) and a much larger component that will be

ejected from the main belt during Phase 2 (N_{dep}, where "dep" stands for dynamically depleted population). Thus, our initial population is $N = N_{\mathrm{rem}} + N_{\mathrm{dep}}$. For CoDDEM, this means separating I_{DISRUPT} into two components:

$$I_{\mathrm{DISRUPT}}^{\mathrm{rem}} = \frac{N_{\mathrm{rem}}}{\tau_{\mathrm{rem}}} + \frac{N_{\mathrm{dep}}}{\tau_{\mathrm{cross}}} \tag{6}$$

$$I_{\mathrm{DISRUPT}}^{\mathrm{dep}} = \frac{N_{\mathrm{dep}}}{\tau_{\mathrm{dep}}} + \frac{N_{\mathrm{rem}}}{\tau_{\mathrm{cross}}} \tag{7}$$

Here τ_{rem} and τ_{dep} describe the collisional lifetimes of objects against disruption events produced by objects in their own respective populations, while τ_{cross} describes the lifetime of objects in N_{rem} against disruption from objects in N_{dep} (and vice-versa). For I_{DYN}, we also define two components: $I_{\mathrm{DYN}}^{\mathrm{dep}}$, which describes the loss of bodies produced in N_{dep} during the DDE, and $I_{\mathrm{DYN}}^{\mathrm{rem}}$, which defines the loss of bodies produced in N_{rem} over solar system history by the Yarkovsky effect/resonances.

Finally, for I_{FRAG}, we assume that ejecta produced by breakup events in N_{rem} and N_{dep} stay within their source populations. This approximation keeps things simple, but it does prevent us from tracking what happens when fragments from a disrupted object in N_{dep} mix with N_{dep} during Phases 1 and 2. This issue is important if one wants to constrain the quantity of highly distinctive taxonomic types found in the main belt (e.g., V-types, M-types, A-types; see Sec. 5.1). This problem will be addressed in the near future using a more specific set of numerical runs.

3.2.2. Computing collision probabilities and impact velocities for CoDDEM

To determine τ_{rem}, τ_{dep}, and τ_{cross} over time, we need to compute the time-varying values of P_i and V_{imp} for the N_{rem} and N_{dep} populations in each of the dynamical phases described in Sec. 3 (see Eq. 3). These values were included in CoDDEM in the form of look-up tables where, at every timestep, they were used to solve Eqs. (6) and (7).

Our procedure was as follows. To compute characteristic P_i and V_{imp} values for bodies within a single population at a single moment in time, or for bodies from two populations crossing one another, the standard technique is to select a representative sample of test bodies from each small body population of interest and then calculate collision probabilities and impact velocities between all possible pairs of asteroids using their osculating (a, e, i) values. In CoDDEM, we did this using the method described by Bottke *et al.* (1994a) (see also Greenberg 1982; Bottke and Greenberg 1993). The possible orbital crossing positions were integrated over uniform distributions of longitudes of apsides and nodes for each projectile-target pair. This approximation is considered reasonable because secular precession randomizes the orientations of asteroid orbits over short timescales ($\sim 10^4$ year). To account for the time-varying (a, e, i) values of the asteroids in our

populations, we computed new values of P_i and V_{imp} across our integration time.

For Phase 1, which extends from the end of accretion to the time of Jupiter's formation, we first needed to extract from the numerical runs described in Sec. 2.2 a test body sample representing N_{rem} and N_{dep}. We did this by defining a "main belt" zone that roughly corresponds to the (a, e, i) location of the observed main belt: $2.0 < a < 3.5$ AU, e values below those needed to reach crossing orbits with the current orbital location of Mars (perihelion $q > 1.66$ AU) or Jupiter (aphelion $Q > 4.5$ AU), and $i < 15°$. Objects evolving out of this zone were considered part of N_{dep}, while those inside were considered part of N_{rem}. Note that our main belt zone parameters exclude some minor parts of the main belt (e.g., the high inclination region that contains asteroid 2 Pallas).

We find that 16 of the original 100 test bodies from Sec. 2.2.1 remain in the main belt zone after 10 My (Fig. 1). To get our N_{rem} sample for Phase 1, the (a, e, i) values of these objects are recorded in a separate file between 0-10 My (in 1 My increments). The same procedure is followed to get our N_{dep} sample, except here we use the 84 bodies outside the main belt zone after 10 My. Using these values and the code in Bottke *et al.* (1994a), we compute P_i and V_{imp} for the N_{rem} sample against themselves, the N_{dep} sample against themselves, and for N_{rem} sample that crosses N_{dep}. The results for each are shown as grey dots in Figs. 6, 7, and 8, respectively.

EDITOR: PLACE FIGURE 6 HERE.

EDITOR: PLACE FIGURE 7 HERE.

EDITOR: PLACE FIGURE 8 HERE.

We follow the same procedure for Phase 2 (Sec. 2.2.2). Here 5 of the original 1000 objects between 2-4 AU were in the main belt zone on stable orbits after 100 My; they comprise our sample for N_{rem}. Even though this sample size is small, we found it did a reasonably good job of reproducing the P_i and V_{imp} values found in the observed main belt (see below). The remaining objects, including the 100 objects started between 1-2 AU, make up our sample for N_{dep}. Note that because 10 times fewer particles were used in the 1-2 AU run, the (a, e, i) values of the test bodies in this sample were cloned 10 times for use in our collision probability/impact velocity code. Our results for P_i and V_{imp} between 10-100 My are shown in Figs. 6, 7, and 8.

The initial conditions for the 100-500 My runs were cloned from the survivors of the N_{dep} sample that lasted 100 My (Sec. 2.2). Tests indicate that test bodies in this set produce P_i and V_{imp} values similar to those found at 100 My. For this reason, we assume the values computed at

100 My extend to the time range between 100-500 My. This also explains why we restrict Figs. 6, 7, and 8 to values between 0-100 My.

An examination of Figs. 6, 7, and 8 shows some jitter in the P_i and V_{imp} values; this is an unavoidable artifact of the limited number of test bodies in our sample. To compensate for this effect, we have fit line segments to the trends shown in the data. The P_i and V_{imp} values used in CoDDEM are taken from these line segments.

For Phase 3, where $N_{dep} = 0$, we use for our N_{rem} sample the set of 682 asteroids with $D > 50$ km (Farinella and Davis 1992; Bottke et $al.$ 1994a). We justify this on the premise that dynamical conditions in the main belt have been essentially unchanged for billions of years. Bottke et $al.$ (1994a) found this set of objects yields $P_i = 2.86 \times 10^{-18}$ km^{-2} yr^{-1} and $V_{imp} = 5.3$ km s^{-1}, values that have been verified by many groups (e.g., Farinella and Davis 1992; Vedder 1998).

The results in Figs. 6, 7, and 8 can be understood by examining the dynamical behavior of the test bodies described in Sec. 2.2. For Fig. 6, we find the N_{rem} sample produced values of $6 < V_{imp} < 8$ km s^{-1} between 0-20 My; they correspond to collisions with the 'square' particles that wandered to high (e, i) values during this interval. Once those particles returned to the main belt zone, P_i and V_{imp} returned to values consistent with those described in Phase 3. For Fig. 8, we find the evolved N_{dep} particles undergo a substantial increase in P_i and V_{imp}. This trend is explained by the fate of the surviving sample, many which have similarly low a and high (e, i) values. The comparable values mean higher collision probabilities; as these particles are eliminated, P_i moves to lower values. Fig. 7 shows the results of N_{rem} striking N_{dep}. As N_{dep} moves to higher (e, i) values, V_{imp} increases as well.

As a caveat, we should point out that we do not know whether the Q_D^* functions used in the paper are appropriate for high velocities ($V_{imp} >> 5$ km s^{-1}). At present, there are no laboratory shot experiments or hydrocode modeling results available to constrain our results. We leave this issue for future work. The interested reader is encouraged to look at appendix in B05 for additional details.

3.3. Computing loss rates produced by dynamical processes

The loss rate described by I_{DYN}^{dep} during the DDE was found using the data described in Fig. 4. At every timestep, we removed a fraction of the N_{dep} population across all size bins based on the number of bodies lost from the Petit et $al.$ (2001) simulations (Sec. 2.2). These bodies were assumed to be lost by falling into a "sink", namely striking a planet (or planetary embryos), impacting the Sun, or being ejected from the inner solar system via a close encounter with Jupiter (Farinella et $al.$ 1994; Gladman et $al.$ 1997). This was continued until the N_{dep} population was eliminated ~ 4.2 Ga.

For I_{DYN}^{rem}, we assumed that objects were lost via the combined perturbations of Yarkovsky

thermal forces and resonances (e.g., Bottke *et al.* 2002a).[2] The Yarkovsky effect is a thermal radiation force that causes asteroids with diameters between $D = 0.01$ m-30 km to undergo semimajor axis drift as a function of their spin, orbit, and material properties. This process drives some of these objects into powerful resonances produced by the gravitational perturbations of the planets (e.g., the 3:1, ν_6 resonances). Numerical studies show that test objects placed in such resonances have their eccentricities pumped up to planet-crossing orbits (e.g., Wetherill and Williams 1979; Wisdom 1983), where they eventually become part of the near-Earth object (NEO) population.

For CoDDEM, we need to determine a Yarkovsky removal rate function representative of the entire main belt population. The structure, nature, and location of the main belt, however, make this challenging work. For example, Bottke *et al.* (2000; 2002b) showed that the inner and central main belt populations ($a < 2.8$ AU) provide $> 80\%$ of the observed NEOs, while the outer main belt has removal rates twice as high as the inner main belt (570 $H < 18$ objects lost per My in the outer main belt vs. 220 $H < 18$ objects lost per My from the inner/central main belt).[3] Comparable differences also show up in the main belt size distribution. Observations from Yoshida and Nakamura (2004) indicate that inner main belt asteroids over a broad H range ($15 < H < 20$) have a slightly steeper power law slope than those in the outer main belt (defined in their paper as $a > 3.0$ AU). This slope difference could be a function of several factors: the non-uniform removal rate functions described above, different population sizes, with many large families located in the outer main belt, and/or different asteroidal physical properties, with the inner main belt dominated by S-type asteroids and the outer main belt by primitive C- /D-type bodies (Gradie and Tedesco 1982; Britt *et al.* 2002).

To resolve this issue for our 1-D model, we focus on the nature of the constraints used by CoDDEM, namely the main belt size distribution reported by Jedicke *et al.* (2002) (see B05 and Sec. 3.4 for details). For the smallest asteroids, this distribution was computed by debiasing asteroid detection statistics. The results, however, can become unavoidably skewed toward easy to detect bodies (e.g., high albedo S-type asteroids in the inner/central main belt) over hard to detect bodies (e.g., low albedo C-type asteroids in the outer main belt); see also Jedicke and Metcalfe (1998). The shape of the size distribution for small asteroids is therefore more likely to be a reflection of the inner/central main belt than the outer main belt. For this and other reasons, we use a removal rate function geared toward inner/central main belt values. This is probably the best we can do until CoDDEM is modified to track the evolution of the inner and outer main belt separately. The interested reader should see O'Brien and Greenberg (2005) for an alternative view

---

[2] We consider the loss of material produced by the Yarkovsky effect/resonances on $N_{\rm dep}$ to be negligible.

[3] Caution should be used when applying the Bottke *et al.* (2002b) outer main belt loss rates to CoDDEM-like codes because no one, as of yet, has realistically quantified the population of dormant comets residing near or in this region. Thus, it is plausible that some of the outer main belt asteroids tracked in the Bottke *et al.* simulations were actually dormant comets.

of this issue.

The actual values in our Yarkovsky removal rate function for $D > 1$ km bodies compare well with numerical results from Morbidelli and Vokrouhlický (2003; hereafter MV03). MV03 modeled the dynamical evolution of asteroids drifting via the Yarkovsky effect all the way from source regions in the inner/central main belt to resonant escape hatches capable of producing NEOs (e.g., ν_6 secular resonance; 3:1 mean motion resonance with Jupiter). They included factors such as collisional disruption, collisional spin axis reorientation events, and the effects of YORP (Rubincam 2000; see also Bottke et al. 2002a). Like MV03, we assumed a size-dependent removal rate for main belt asteroids in each size bin, with a linear decrease from 0.03% per My for $D = 1$ km bodies to 0.008% per My for $D = 10$ km bodies. This trend continues to 0.005% per My for $D = 20$ km bodies and 0.0002% per My for $D = 30$ km bodies. Beyond this point, we assume little escapes the main belt.

For $D < 1$ km bodies, our removal rate model is uncertain, with little trustworthy numerical work done on this issue to date. To glean insights into plausible values, we compared the main belt population from B05 between $D = 10$ cm to 1 km to the known NEO population (and various constraints) over the same size range (Stokes et al. 2003; Stuart and Binzel 2004; see Secs. 5.2 and 5.4). Remarkably, we found both populations shared the same essential shape.

How realistic is this match, and can the main belt at small asteroid sizes be significantly shallower or steeper than predicted by B05? For the NEO population, we now have reasonable constraints over a range of sizes down to $D \sim 10$ cm (see Sec. 5.4). For the main belt, the shape of its size frequency distribution for $D < 0.2$ km asteroids is a function of the slope of Q_{D}^* in the strength regime (O'Brien and Greenberg 2003). The more shallow/steep Q_{D}^* is in the strength regime, the more shallow/steep the slope for $D < 0.2$ km asteroids. B05 found only a small number of Q_{D}^* shapes could reproduce both main belt and laboratory shot experiment constraints, with the shape of Q_{D}^* in the gravity-regime producing most of the uncertainty. In the end, B05's best fit Q_{D}^* model was found to be an excellent match with those found in hydrocode experiments (e.g., Benz and Asphaug 1999); this suggests their estimate of the main belt size distribution from $D = 10$ cm to 0.2 km was also reasonable. Thus, unless our interpretation of laboratory shot data is inaccurate and/or our understanding of small body disruption events are faulty, we can only infer that the similarity between the main belt and NEO populations is no accident.

This affinity between these two size distributions has consequences for our Yarkovsky loss rates. To reproduce the NEO population (see Secs. 5.2 and 5.4), we were forced to adopt the same removal rate for sub-km asteroids (10 cm $< D < 1$ km) as $D \sim 1$ km asteroids (0.03% per My). These values assume the average NEO has a residence time of ~ 4 My. The lifetime was computed using the average lifetimes of test bodies in each main belt source region combined with the relative importance of each source (Bottke et al. 2002b). Note that our computation did not use the Bottke et al. flux rates from each source (O'Brien and Greenberg 2005), so our NEO lifetime, like our main belt population, is skewed toward the inner/central main belt region where

most observable NEOs originated.

Our Yarkovsky/resonance loss rates differ from results one might expect from more idealized estimates (e.g., Farinella *et al.* 1998; Bottke *et al.* 2000). We caution that idealized Yarkovsky drift rates may not be appropriate in this context, because they do not account for (i) how asteroidal thermal conductivity changes with asteroid size, (ii) how asteroid lifetimes change with size, (iii) how YORP affects the spin vectors and thus the Yarkovsky drift rates of small asteroids (Rubincam 2000; Vokrouhlický and Čapek 2002), and (iv) how the small body population bordering main belt resonances changes with time. Much work on this topic remains to be done.

We assume our NEOs undergo zero comminution, a simple approximation we believe reasonable given the dynamical structure of the NEO population. Most NEOs fresh from the main belt have short dynamical lifetimes ($\lesssim$ 1 My), with only a small fraction ever making it to $a < 2$ AU (Bottke *et al.* 2002b). Long-lived NEOs (dynamical lifetimes of tens of My), however, tend to have orbits that keep them away from the main belt. Thus, for the former, collisional lifetimes are of reduced importance, while for the latter, collisional lifetimes are several orders of magnitude longer than typical main belt asteroids (Bottke *et al.* 1994b). As before, the greatest uncertainty in our approximation is at small sizes.

3.4. Model Constraints

The primary constraints used in CoDDEM are described in B05. We briefly review them below.

Constraint #1: The main belt size frequency distribution.

The first CoDDEM constraint comes from the observed main belt size frequency distribution. As described in B05, we derive this function using the absolute magnitude H distribution provided by Jedicke *et al.* (2002), who combined results from the Sloan Digital Sky Survey (SDSS) for $H > 12$ (Ivezić *et al.* 2001) with the set of known main belt asteroids with $H < 12$. To transform the H distribution into a size distribution, we use the following relationship between asteroid diameter D, absolute magnitude H, and visual geometric albedo p_v (e.g., Fowler and Chillemi 1992):

$$D = \frac{1329}{\sqrt{p_v}} 10^{-H/5}. \tag{8}$$

where p_v was set to 0.092. The only other change made to the Jedicke *et al.* distribution was to include the observed asteroids for $D > 300$ km using the IRAS/color- albedo-derived diameters cited in Farinella and Davis (1992). The cumulative number of asteroids with $D > 1, 50$ and 100 km obtained from our population was 1.36×10^6, 680, and 220, respectively, in agreement with several published population estimates (e.g., Farinella and Davis 1992; Tedesco and Desert

2002; Morbidelli and Vokrouhlický 2003).

We see that the main belt size frequency distribution is wavy, with "bumps" near $D \sim 3$-4 km and one near $D \sim 100$ km. Several groups have shown that the second bump is a by-product of collisional evolution, with a wave launched by a change in slope near $D = 200$ m between strength- and gravity-scaling disruption regimes (Campo Bagatin $et\ al.$ 1994; Durda $et\ al.$ 1998; O'Brien and Greenberg 2003; see Davis $et\ al.$ 2002 for a recent review). As asteroids increase in size, changes from negative Q_{D}^* slopes in the strength regime to positive slopes in the gravity regime mean that asteroids just beyond the inflection point become more difficult to disrupt. Because these objects live longer, more of them survive, which in turn creates an excess number of projectiles capable of disrupting larger asteroids. This perturbation launches a wavy pattern into the size distribution and creates a bump near $D \sim 3$-4 km. B05 show the larger bump near $D \sim 100$ km is likely a byproduct of accretion in the primordial main belt.

Constraint # 2: Asteroid families.

A second set of constraints was provided by asteroid families, which are the remnants of catastrophic collisions in the main belt (e.g., Zappalà $et\ al.$ 2002). They are identified by their clustered values of proper semimajor axes a, eccentricities e, and inclinations i (Milani and Knežević 1994; Bendjoya and Zappalà 2002, Knežević $et\ al.$ 2002). B05 focused on families produced by the disruption of $D > 100$ km parent bodies. These families have members that are too large to be dispersed by the Yarkovsky effect or ground away by comminution over several Gy (Nesvorný and Bottke 2004; Nesvorný $et\ al.$ 2004).

To determine how many families fit this criteria, B05 used hydrocode simulations of asteroid collisions (Durda $et\ al.$ 2004) to estimate the amount of material in each family located below the observational detection limit. They then used their results to compute the parent body diameter for each family. B05's results suggest that ~ 20 families have been produced by the breakup of $D \gtrsim 100$ asteroids over the last ~ 3.5 Gy. The value 3.5 Gy was used as an age limit because the dynamical instability that produced the LHB (Levison $et\ al.$ 2001; Gomes $et\ al.$ 2004) would have also scrambled our ability to compute useful proper (a, e, i) elements beyond this epoch (see B05 and Sec. 2.2.4 for details). Note that changing this value to 4.6 Ga would only introduce a $\sim 20\%$ error into our estimate. Accordingly, we assume that the incremental size bins in N_{rem} centered on $D = 123.5, 155.5, 195.7, 246.4, 310.2$, and 390.5 km experienced 5, 5, 5, 1, 1, 1 breakups over the last 3.5 Gy, respectively. Given the width of these bins, our CoDDEM runs should produce reasonable results even if there are moderate uncertainties in the size of each family's parent body.

Constraint # 3: The intact basaltic crust of (4) Vesta.

Asteroid (4) Vesta ($D = 529 \pm 10$ km; Thomas $et\ al.$ 1997; Standish 2001; see Britt $et\ al.$ 2002), is the only known differentiated asteroid in the main belt. Evidence from the HED meteorites indicates Vesta differentiated and formed its 25-40 km crust ~ 6 My after the formation of the first solids (i.e., CAIs) (e.g., Shukolyukov and Lugmair 2002). The surface of Vesta is dominated by the presence of a $D = 460$ km impact basin. This basin is believed to have formed from the

impact of a $D \sim 35$ km projectile and is likely the source of the Vestoids, V-type multikilometer asteroids that populate the inner main belt and share the same inclination at Vesta (Marzari *et al.* 1996; Thomas *et al.* 1997; Asphaug 1997). The singular nature of this crater can be used to set limits on the frequency of impacts in both the primordial and present-day main belt.

Constraint # 4: The lunar and terrestrial impactor flux over the last 3 Gy.

A fourth constraint comes from the estimated lunar and terrestrial cratering rates, which appear to have been relatively constant (within a factor of 2) over 0.5-0.8 to 3 Ga (e.g., Grieve and Shoemaker 1994; Shoemaker and Shoemaker 1996; McEwen *et al.* 1998; Shoemaker 1998). Because most NEOs come from the main belt via the Yarkovsky effect (Bottke *et al.* 2002a,b), the impactor flux on the Earth and Moon provides information on how the main belt size distribution has changed over time. This result implies the NEO population over the $D < 30$ km size range (and thus the main belt population) has been in a quasi-steady state over this time period. Some groups claim there has been a factor of 2 increase in the impact flux over the last 120 Ma (e.g., Grieve and Shoemaker 1994; Neukum and Ivanov 1994; S. Ward, personal communication). Others claim this change occurred over the last 400-800 Ma (McEwen *et al.* 1998; Culler *et al.* 2000), though this is considered controversial (Hörz 2000; Grier *et al.* 2001; see B05 for details).

Additional Constraints

Our estimated collisional lifetimes for main belt asteroids can also be tested against the cosmic ray exposure ages of stony meteorites (e.g., Marti and Graf 1992; Eugster 2003), fireball data (Morbidelli and Gladman 1998), and collisional activity within the Koronis family (Vokrouhlický *et al.* 2003). These issues are discussed in Sec. 5.2.

One potential constraint we do not use is the NEO population, mainly because our Yarkovsky removal rate model was designed to reproduce it from the observed population. Nevertheless, we can use our results to gain several important insights into the shape and nature of the NEO population. These issues are discussed in Sec. 5.4. We also do not test our results against the crater histories of the observed asteroids at this time. A few of our reasons are as follows: (i) the cratered surfaces of (243) Ida, (253) Mathilde, and (433) Eros are close to saturation equilibrium (e.g., Chapman 2002); (ii) "old" and "new" craters on (951) Gaspra show different power law slopes; (iii) the crater scaling relationships needed to convert projectiles into craters on asteroid surfaces, let alone planetary surfaces, is not well understood (see Sec. 5.5); and (iv) crater records on asteroid surfaces have probably been influenced by crater erasure mechanisms and the stochastic nature of large impact events (e.g., Greenberg *et al.* 1994; 1996; Richardson *et al.* 2004).

4. Model Runs

4.1. Initial conditions

In this section, we describe the input parameters needed by CoDDEM to track the evolution of the main belt. The principal unknowns affecting the DDE in our model are the timescale of Jupiter's formation and the initial size distribution of the main belt population. Using results from B05, we assume the *shape* of the latter is constrained to a fairly narrow range of values, though its magnitude is treated as a free parameter. Another important unknown extensively investigated by B05 is the asteroid disruption scaling law Q_D^*. We limit our tests of Q_D^* to a range of functions around B05's best fit values (e.g., Fig. 5).

Our initial size frequency distribution is defined in terms of N_{rem} and N_{dep}. We assume the starting N_{rem} population is similar to that described by B05. For $D > 200$ km, we use the same number of objects as the observed main belt asteroids, with a few objects added in to account for the breakup of large asteroids over 4.6 Gy (e.g., parent bodies of the Eos and Themis families). For $D_x < D < 200$ km, where D_x is an inflection point, the population follows a differential power law index of -4.5, a value close to the observed slope of asteroids in this size range. For $D < D_x$, we follow a shallow slope of -1.2. We treat D_x here as an unknown. B05 tested $D_x = 80$, 100, and 120 km, with the best fit to main belt constraints found for $D_x = 120$ km. Here we limit our search to values close to the best fit case of B05, namely $D_x = 100$, 105, 110, 115, and 120 km (Fig. 9). Our size range of interest extends from meter-sized bodies to Ceres-sized objects.

We set $N_{dep} = fN_{rem}$, where f is an integer between 50 and 600. This range brackets the removal rates found in Petit *et al.* (2001). Because N_{rem} is comparable to the current main belt's mass ($\sim 5 \times 10^{-4} M_\oplus$), f can also be thought of as the number of main belt masses in N_{dep}. As a handy rule-of-thumb, one can assume that $100 \times N_{rem}$ is approximately the same as 4 lunar masses, 0.5 Martian masses, or $0.05 M_\oplus$. The remaining mass in the primordial main belt population is assumed to be contained in Moon-to-Mars-sized embryos.

EDITOR: PLACE FIGURE 9 HERE.

The time of Jupiter's formation relative to the onset of fragmentation in the main belt, (t_{Jup}) is assumed to be between 1 and 10 My (Haisch *et al.* 2001). As shown in Sec. 2.2, a full-grown Jupiter has a dramatic effect on the values of P_i, V_{imp}, and the dynamical removal rate N_{loss} in the main belt. Hence, when CoDDEM reaches $t = t_{Jup}$, we jump from Phase 1 to Phase 2 values in P_i, V_{imp}, and N_{loss} (i.e., the values seen on Fig. 4, Figs. 6, 7, and 8 for $t_{Jup} = 10$ My). We believe this approximation is reasonable because our Phase 2 dynamical model (from Petit *et al.* 2001) indicates the dynamical excitation produced by Jupiter/embryos essentially dominates any prior excitation produced by the embryos alone.

4.2. Demonstration cases

Here we show several sample CoDDEM results. Fig. 10 shows six snapshots from a test run where $f = 200$ (i.e., the initial population is ~ 200 times the size of the current main belt), $D_x = 110$ km (Fig. 9), and $t_{\mathrm{Jup}} = 4$ My. The total simulation time was 4.6 Gy. The Q_{D}^* function was set to mimic results provided by the hydrocode results of Benz and Asphaug (1999), with Eq. (5) parameters $E = 0.866, F = -0.895, G = -0.495,$ and $H = -0.303$. The $t = 0$ My timestep displays the initial conditions for the N_{rem} and N_{dep} populations (solid and dot-dashed lines, respectively). The observed main belt size distribution is shown as black dots.

EDITOR: PLACE FIGURE 10 HERE.

Collisional evolution prior to the formation of Jupiter (Phase 1) is represented by the $t = 3$ My timestep. We see that comminution generates a bump near $D \sim$ 3-4 km for both N_{rem} and N_{dep}. As explained by several authors (e.g., Campo Bagatin *et al.* 1994; Durda *et al.* 1998; Davis *et al.* 2002; O'Brien and Greenberg 2003; B05), this bump is a by-product of the "V"-shaped Q_{D}^* function, where a perturbation is induced by a change between strength- and gravity-scaling regimes near $D = 0.2$ km (Fig. 5). At still smaller sizes, the main belt enters into a Dohnanyi-like collisional equilibrium (Dohnanyi 1969), with a differential power law index of -3.6 set by the slope of the Q_{D}^* function in the strength regime (O'Brien and Greenberg 2003). This power law index value is unlikely to stay constant to extremely small sizes, however, because $D \lesssim 1$ cm bodies are susceptible to Poynting-Robertson drag (e.g., Dermott *et al.* 2002).

For $t_{\mathrm{Jup}} > 4$ My (Phase 2), N_{dep} is ejected from the main belt by the combined perturbations of Jupiter and planetary embryos. The loss of bodies from N_{dep} via dynamical effects is seen in timesteps $t = 10, 30$ and 100 My. At the same time, impacts on N_{rem} from N_{dep} and, to a lesser degree, from N_{rem} continue to reshape it, enough that after 30 My it approximates the shape of the current main belt. Even so, comminution among N_{rem} asteroids for another ~ 4.5 Gy (Phase 3) is needed to reproduce our constraints. Note that this evolutionary pattern can differ from case to case; some trials reproduce the shape of the main belt at early timesteps only to lose it at 4.6 Gy, while in other cases only attains the appropriate shape at the end of the simulation. This variability is driven by the stochastic nature of breakups in the main belt.

To quantify the fit between the model and observed population, we follow the methods described by B05. The first metric used compares the shape of the model population to a small envelope of values surrounding the observed main belt population (defined as N_{MB}):

$$\psi_{\mathrm{SFD}}^2 = \sum_D \left(\frac{N_{\mathrm{rem}}(D) - N_{\mathrm{MB}}(D)}{0.2 N_{\mathrm{MB}}(D)} \right)^2 \tag{9}$$

Tests indicate that $\psi_{\mathrm{SFD}}^2 < 20$ generally provides a good match between model and data. The 6 snapshots shown in Fig. 10 have ψ_{SFD}^2 values of 372, 335, 237, 23.5, 24.4, and 9.3 for

$t = 0, 3, 10, 30, 100$, and 4600 My, respectively. The only value that counts for our ψ^2_{SFD} metric is the last one.

The second test is a standard χ^2 test (Press *et al.* 1989) used to compare the number of breakups produced in our model against the constraints provided by asteroid families. At $t = 4.6$ Gy, we compute the number of destroyed bodies in each $D > 100$ km size bin ($\Delta N_{\mathrm{disrupt}}$) over the last 3.5 Gy (see B05) and compare that value to the observed number of families in every size bin with $D > 100$ km (Sec. 3.4). We assume a good fit between model and data is one where the value obtained, χ^2_{FAM}, is better than 2σ (i.e., probability $> 5\%$). Note that this value is more relaxed than that described by B05; we do this because we compare model results with data for a single moment in time, whereas B05 allowed their model fits to occur at anytime over a pseudo-time interval of 50 Gy. For Fig. 10, χ^2_{FAM} yields a probability $> 78\%$, with 6, 4, 3, 2, 1, and 0 disruption events in the incremental size bins centered on $D = 123.5, 155.5, 195.7, 246.4, 310.2$, and 390.5 km, respectively, over the last 3.5 Gy.

The steady state number of $D > 1$ km NEOs estimated from this trial case is ~ 1100, the same as that predicted by Stokes *et al.* (2003) (see also Stuart 2001 and Stuart and Binzel 2004). We find that strengthening or weakening our Yarkovsky removal rate function produces a mismatch with the observed NEO population (see Sec. 5.4). Only significant increases in our loss rates, however, visually affect the main belt size distribution. See Sec. 3.3 for details.

Our results indicate that the main belt and NEO populations entered into a quasi-steady state during the last ~ 3 Gy, with both SFDs remaining essentially constant except for small (within a factor of about 2) variations among the $D < 10$ km asteroids. The largest increases in both populations were produced in the immediate aftermath of large-scale disruption events (e.g., $D \gtrsim 200$ km), which led to a surge of new main belt asteroids and NEOs. Low population values occurred when long intervals passed between such disruption events. This steady state explains why crater production rates on the Earth and Moon have been relatively constant over the last 3 Gy (e.g., Shoemaker 1998).

There are several common failure modes for our CoDDEM trials, two of which are shown in Fig. 11. In Fig. 11a, we used the same parameters as those above except we varied the nature of the DDE by setting $t_{\mathrm{Jup}} = 1$ My and $f = 50$. With N_{dep} set to a small value and the DDE occurring early, Phase 1 and 2 comminution produced relatively limited damage to the N_{rem} population. Hence, at $t = 4.6$ Gy, the model population is still short of the observed population ($\psi^2_{\mathrm{SFD}} = 30.6$). The steady state number of $D > 1$ km NEOs is ~ 780, about 30% short of the Stokes *et al.* (2003) predictions. Interestingly, χ^2_{FAM} yields a probability $> 27\%$, a success by our 2σ criteria, with 5, 7, 2, 2, 0, and 0 disruption events over the last 3.5 Gy in the incremental size bins centered on $D = 123.5, 155.5, 195.7, 246.4, 310.2$, and 390.5 km, respectively. This match can be explained by inspecting Fig. 11a; because N_{dep} projectiles did little damage to the N_{rem} population, Phase 3 comminution was able to reproduce the observed distribution of asteroid families.

For Fig. 11b, we set $t_{\rm Jup} = 10$ My and $f = 600$. Hence, the equivalent of $0.3 M_\oplus$ of material was placed into the $N_{\rm dep}$ population, all in bodies the same size or smaller than asteroid (1) Ceres. When combined with an abundance of Phase 1 comminution produced by a late-forming Jupiter, we find that $N_{\rm dep}$ decimates the $20 < D < 100$ km population in $N_{\rm rem}$ before disappearing. Consequently, $N_{\rm rem}$ never recovers; $\psi^2_{\rm SFD} = 31.3$ for this trial case at $t = 4.6$ Gy. Moreover, $\chi^2_{\rm FAM}$ yields a probability of 2.6×10^{-9}, with 4, 0, 0, 1, 1, and 0 disruption events over the last 3.5 Gy in the incremental size bins centered on $D = 123.5, 155.5, 195.7, 246.4, 310.2$, and 390.5 km, respectively. These results indicate that there are real limits to the length of the DDE and to the size of the $N_{\rm dep}$ population.

<div align="center">EDITOR: PLACE FIGURE 11 HERE.</div>

These runs assume the $Q^*_{\rm D}$ functions derived by B05 are applicable in all the impact velocity regimes experienced by the $N_{\rm rem}$ and $N_{\rm dep}$ populations. At present, we have no data to test whether this approximation is valid, particularly for $V_{\rm imp} > 10$ km s^{-1}. It appears, however, that high velocity impacts do not have a dominant effect on main belt comminution, mainly because these velocities become important only after the $N_{\rm dep}$ population has been significantly depleted. Nevertheless, we believe deriving a useful $Q^*_{\rm D}$ function for high speed impacts is an important area for future work by impact modelers.

4.3. Production runs and results

With these endstates in mind, we can now discuss our CoDDEM production runs. We define a "run" to be 100 trial cases executed with different random seeds over a given set of $(t_{\rm Jup}, f, D_x, Q^*_{\rm D})$ parameters. The large number of trials was necessary to properly determine how stochastic breakup events affect the final results; recall that breakup events in CoDDEM are determined using random deviates and Poisson statistics. For each trial case, we compared our model results with our constraints after 4.6 Gy of evolution. Positive matches were defined by $\psi^2_{\rm SFD} < 20$ and $\chi^2_{\rm FAM} < 2\sigma$ (i.e., probability $> 5\%$).

Unfortunately, while CoDDEM is an efficient code, we lacked the computational resources to execute runs over a wide and uniformly-spaced matrix of $t_{\rm Jup}, f, D_x$, and $Q^*_{\rm D}$ values. Instead, we explored a representative set of parameters across this matrix. We started by setting the $Q^*_{\rm D}$ function to the Benz and Asphaug (1999) function described in Sec. 3.1 (i.e., #13 on Fig. 5). Next, we ran CoDDEM over a matrix of $(t_{\rm Jup}, f, D_x)$ values, with $t_{\rm Jup} = 1\text{-}10$ My (values incremented by 1 My), $f = 50\text{-}600$ (values incremented by 50), and $D_x = 100, 105, 110, 115$ and 120 km. Thus, this initial set of 600 runs consisted of 60,000 CoDDEM trial cases run with different random seeds.

An analysis of our results suggests that $D_x = 110$ km was the best performer, with 31, 15, and 4 of the $(t_{\rm Jup}, f)$ runs (out of possible 120) having a success rate greater than 30%, 35%, and

40%, respectively. To say this another way, 4 of the $D_x = 110$ km runs, each composed of 100 trial cases, had more than 40 trial cases that matched our ψ^2_{SFD} and χ^2_{FAM} criteria. The next best performer was $D_x = 105$ km, with 26, 7, and 1 of their (t_{Jup}, f) runs having a success rate larger than 30%, 35%, and 40%, respectively. No other D_x values beat the 40% mark, and $D_x = 115$ km only attained $> 35\%$ once out of 120 runs. We infer from this that the most likely inflection point for our initial main belt size distribution is $D_x = 110$ km.

Our predicted $D_x = 110$ km value is slightly smaller than the best fit $D_x = 120$ km value estimated by B05, though it must be said that B05 only tested $D_x = 80, 100,$ and 120 km. We believe $D_x = 120$ km was less successful in our CoDDEM tests because a non-trivial number of $20 < D < 100$ km objects were disrupted via high impact velocities during the DDE. By definition, the method used by B05 could not account for these effects.

For our next set of tests, we kept $D_x = 110$ km constant and investigated the Q^*_{D} functions #7-14 shown in Fig. 5 across a matrix of (t_{Jup}, f) values This set was chosen by testing the Q^*_{D} functions adjacent to #13 and then iterating until we were convinced we had found the peak values in our runs. Together, our tests comprised 960 runs and 96,000 CoDDEM trial cases.

The best performer among our Q^*_{D} function tests was #10, with Eq. (5) parameters of $E = 0.873, F = -0.868, G = -0.486,$ and $H = -0.297$ (gold curve in Fig. 5). We found that 36, 14, 7, and 2 of the (t_{Jup}, f) runs (out of possible 120) had a success rate greater than 30%, 35%, 40%, and 45%, respectively. The next closest, #9, was nearly as good, with 34, 15, 5, and 2 runs having a success rate greater than 30%, 35%, 40%, and 45%, respectively. Its parameters were $E = 0.881, F = -0.840, G = -0.476,$ and $H = -0.290$. The other Q^*_{D} functions tested were less successful, with none having a run with a success rate $> 45\%$. The Q^*_{D} functions #11, #12, and #13, however, did have 3-4 runs with a success rate $> 40\%$.

Our best fit Q^*_{D} function #10 is slightly shallower than the Q^*_{D} function determined by Benz and Asphaug (1999), who used smoothed particle hydrodynamics (SPH) codes to determine the impact energy needed for basaltic projectiles to blast apart undamaged basaltic asteroids. They are surprisingly compatible, however, with recent SPH experiments where the target bodies were given highly fractured internal structures (P. Michel, personal communication). Thus, our best fit Q^*_{D} function may be telling us that pre-damaged target bodies are a better analogue for real asteroids than undamaged target bodies. This is consistent with the idea that fracturing or shattering events are much more likely to take place than disruption events (e.g., Asphaug *et al.* 2002).

Taking $D_x = 110$ km and Q^*_{D} function #10, we executed a detailed series of 560 runs over (t_{Jup}, f) with $t_{\text{Jup}} = 1$-10 My (values incremented by 1 My) and $f = 50$-600 (values incremented by 10). The total number of trial cases was 56,000. Our results are shown in Fig. 12, where the contours represent the number of trial cases (out of 100) in each run that met our constraints.

EDITOR: PLACE FIGURE 12 HERE.

Table 1 lists the (t_{Jup}, f) runs where our constraints were met by $\geq 40\%$ of the 100 trial cases. An analysis of these 19 data points provides several interesting results. For example, while the peak value in Fig. 12 is at $(t_{\mathrm{Jup}} = 10$ My, $f = 110)$, approximately 80% of the Table 1 runs have t_{Jup} between 1-4 My. The minimum and maximum f values for the $1 \leq t_{\mathrm{Jup}} \leq 4$ My values, as well as all Table 1 data, are 70 and 230, respectively. The mean and median values of t_{Jup} from Table 1 values are 3.3 ± 2.6 My and 2 My, respectively, while the mean and median values of f are 160 ± 44 and 150, respectively. Though there is some scatter, a line fit to Table 1 data yields the equation $f = 186$ My $- 8.2 \times t_{\mathrm{Jup}}$.

EDITOR: PLACE TABLE 1 HERE.

The runs with smaller success rates predominately have trial cases that fall into one of the two failure modes shown in Fig. 11. For small f and t_{Jup} values, there tends to be too little comminution to reproduce the main belt size distribution. For large f and t_{Jup} values, N_{dep} does too good a job of destroying objects between $20 < D < 100$ km (see Fig. 11b); once these objects are obliterated, the main belt size distribution never recovers. Still, it is important to note that just because the success rate for a given run is low does not mean it could not happen. Until additional constraints become available, we cannot rule out the possibility that current main belt conditions are a statistical fluke produced by the timely breakup of a few large asteroids.

Assuming that our best fit values are telling us something about main belt history, we infer that the primordial main belt for $D \lesssim 1000$ km planetesimals once contained $\sim 70\text{-}230$ times the mass of the current main belt. The most likely values correspond to the central part of this range. This translates into $0.035\text{-}0.11 M_\oplus$, a small fraction of the total mass that is thought to have once existed in the main belt zone during planet formation (Weidenschilling 1977). The remaining mass would need to be in the form of planetary embryos. Our results are similar to back-of-the-envelope calculations made by B05. They are also consistent with the dynamical results of Petit *et al.* (2001), who found that $\sim 0.005\%$ of the test bodies initially emplaced in the primordial main belt would survive the DDE.

Even though our model results suggest that Jupiter's formation could have occurred at nearly any time between 1-10 My, the most likely scenario is that Jupiter formed at $t_{\mathrm{Jup}} \leq 4$ My (average value of 3.3 ± 2.6 My). We assume $t_{\mathrm{Jup}} = 0$ My is when fragmentation started among the $D \lesssim 1000$ km planetesimals. These results are in good agreement with the estimated mean disk lifetime of 3 My predicted by Haisch *et al.* (2001).

5. Discussion and Implications

Here we briefly outline the issues discussed in this section. In Sec. 5.1, we explore the disruption history of the main belt and speculate on the possible origin of asteroids believed to be

derived from differentiated parent bodies (e.g., M-type asteroid 16 Psyche; V-type asteroid 1459 Magnya). In Sec. 5.2, we compare our predicted collisional lifetimes to the cosmic ray exposure ages of stony meteorites and to other lifetime estimates in the literature. In Sec. 5.3, we compare our results to the crater history of asteroid 4 Vesta. In Sec. 5.4, we compare our predictions for the NEO population to observational data. As a follow-up, we discuss in Sec. 5.5 whether small craters on Mercury, Mars, and the Moon are more likely to be primaries or secondaries. Finally, in Sec. 5.6, we review some of the meteoritical evidence for an early comminution phase in the primordial main belt.

The interested reader should also turn to B05, where we compare our results to asteroid spin rate and lightcurve amplitude data. Our results suggest that most $D \gtrsim$ 100-120 km asteroids are primordial, with their spin rates and shapes set by processes occurring during or shortly after accretion. As we go to smaller sizes, main belt asteroids become increasingly dominated by collisional fragments. This change may explain the inflection point seen in the distribution of rotation periods and lightcurve amplitudes near $D \sim 100$ km.

5.1. Disruption history of main belt asteroids

In our CoDDEM runs, we tracked the number of catastrophically disrupted objects in each size bin over 4.6 Gy. A sample of our results are shown in Fig. 13, where the data is taken from the Table 1 run with $t_{\rm Jup} = 3$ My, $f = 180$, $D_x = 110$ km, and $Q_{\rm D}^*$ function #10. The points on Fig. 13 represent the number of disrupted bodies in each size bin that have been summed and averaged over the 44 trials that matched our constraints. The symbols describe those values at 3, 10, 100, and 4600 My. The points connected by the dotted line represent disrupted asteroids from the $N_{\rm dep}$ population, while those connected by the solid line are from $N_{\rm rem}$. Overall, we found that the number of breakups occurring after the DDE is consistent with the predictions of B05 (e.g., $D \sim 30$ km bodies disrupt every ~ 20 My). They differ from previous estimates (e.g., Burbine *et al.* 1996; Marzari *et al.* 1999; see B05 for a review), though we believe our results are better constrained than previous efforts. For more on asteroid lifetimes, see Sec. 5.2.

EDITOR: PLACE FIGURE 13 HERE.

If these results reflect reality, they provide important insights about how the asteroid belt reached its current state. We see that at $t_{\rm Jup} = 3$ My, just prior to the formation of Jupiter and the DDE, the cumulative number of $D > 100$ km bodies disrupted in the $N_{\rm dep}$ population was ~ 500, while the number of disrupted Vesta- and Ceres-sized objects ($D \gtrsim 450$) was ~ 7. These results imply that many large asteroids, some of which may have been differentiated, disrupted early in solar system history. Because these disruption events produced numerous fragments, it is probable that some portion of the parent body survived the DDE. Note that while CoDDEM does not track mixing between the $N_{\rm rem}$ and $N_{\rm dep}$ populations, a significant amount had to occur.

Thus, the $N_{\rm rem}$ population at the beginning of Phase 3 should have been composed of a relatively small number of intact $D \gtrsim 100$ km objects as well as numerous $D \lesssim 100$ km fragments produced by Phase 1 and 2 disruption events in both $N_{\rm rem}$ and $N_{\rm dep}$.

How many different parent bodies currently exist in the current main belt population? The answer depends on the timing of various disruption events as well as the efficiency of mixing that occurred in Phases 1 and 2. For example, Fig. 13 shows that a large number of disruption events in $N_{\rm dep}$ occurred after the formation of Jupiter. We estimate that the $N_{\rm dep}$ population experienced 20-40 times the degree of comminution during the DDE compared to that before it. It is plausible that fragments in this population may have become trapped in the main belt zone by gravitational interactions with planetary embryos. Figs. 2 and 3, however, suggest that the efficiency of this type of mixing was limited. Addressing this issue quantitatively will require a more specific set of numerical runs than described in this paper. (For a recent review of the number of parent bodies represented in our meteorite record, see Burbine *et al.* 2002).

We hypothesize that the survival of fragments from disrupted parent bodies in Phases 1 and 2 could explain the ubiquitous but limited presence of main belt asteroids that appear to be fragments of differentiated parent bodies. When a differentiated asteroid disrupts, it is thought to produce several different asteroid taxonomic types: M-types, iron-rich asteroids that come from the core, A-types, olivine-rich metal-free silicate asteroids that come from the mantle, and V-types, basalt-rich asteroids that come from the crust. Note that Keil (2002; see also Wilson and Keil 1991) predicts the last type may be exceedingly rare because basaltic lava on small differentiated bodies may have had enough entrained gas to reach escape velocities during eruption. Assuming these fragments were produced before or immediately after the formation of Jupiter, a small fraction may have survived the DDE to reach the $N_{\rm rem}$ population. This may explain the relative paucity of these fragments in the observed main belt population.

An example of a V-type fragment produced by a disrupted differentiated body may be (1459) Magnya, a $D = 30$ km V-type asteroid located in the outer main belt. Visible and near-infrared spectroscopic observations indicate that Magnya has a basaltic surface similar to Vesta's crust, but dynamical models suggest there is no association between this object and Vesta (Lazzaro *et al.* 2000; Michtchenko *et al.* 2002). More examples could be the 22 A-type asteroids identified by the SMASS and SMASSII surveys (out of a total sample of 950), with the largest body having $D \sim 60$ km (Xu *et al.* 1995; Bus and Binzel 2002a,b). Finally, asteroids (16) Psyche and (216) Kleopatra ($D = 250$ and 120 km, respectively), M-type asteroids with radar albedos consistent with their surfaces being dominated by material analogous to iron meteorites (Magri *et al.* 1999; 2001), potentially could be explained by the dynamical survival of a few exposed cores produced prior to the DDE (e.g., Davis *et al.* 1999).[4]. To confirm our hypothesis, we will need to explore

[4]Supporting evidence that (16) Psyche is an exposed iron core comes from Kuzmanoski and Kovačević (2002), who used Psyche's perturbations on asteroid (13206) 1997GC22 to estimate a bulk density of 6.98 ± 0.58 g cm^{-3}. Kuzmanoski and Kovačević (2002) claim their work supersedes lower bulk density estimates (e.g., Viateau 2000),

several issues that are beyond the scope of this paper (e.g., How many differentiated asteroids resided in the primordial main belt? What is the probability that a parent body capable of producing Psyche would have disrupted before or during the DDE? What is the probability that a Psyche-like object would have survived the DDE when only 1 in ~ 200 objects survives the DDE?).

Given the lack of evidence for intact differentiated bodies (other than Vesta) in the main belt, it is likely that few such objects ever existed in the primordial main belt. Note that to date, asteroid families show little indication that their parent bodies were differentiated (e.g., Cellino *et al.* 2002). To solve this quandary, we hypothesize that some differentiated fragments may not be indigenous to the main belt, but instead may have been scattered there from $a < 2$ AU orbits by planetary embryos (e.g., Wasson and Wetherill 1979). This issue will be further investigated in a future paper.

5.2. Asteroid collisional lifetimes and disruption intervals

Another way to test our CoDDEM results is to examine the collisional lifetimes (τ) predicted by our model at 4.6 Gy and compare them to the available data. Fig. 14 shows the collisional lifetime of current main belt objects according to our code. For comparison, we have also plotted the collisional lifetime estimate of Farinella *et al.* (1998) ($\tau = 16.8\,\mathrm{My} \times \sqrt{R(\mathrm{m})}$). Our function yields $\tau \sim 14$ My for $D = 1$ m bodies, a value that agrees with the cosmic ray exposure ages of stony meteorites across many different classes (Marti and Graf 1992; Eugster 2003) and with Farinella *et al.* (1998).

EDITOR: PLACE FIGURE 14 HERE.

For $D = 1$-10 cm objects, we obtained $\tau = 3$-6 My. These values are consistent with results from Morbidelli and Gladman (1998), whose dynamical investigation of fireballs data suggested such objects disrupt ~ 3 My after leaving the main belt. Note that objects evolving out of the main belt onto NEO orbits have impact velocities with main belt material of ~ 10 km s^{-1}, twice as high as impact velocities inside the main belt (Bottke *et al.* 1994b). These higher velocities would decrease the lifetimes of the larger fireballs, enough to allow them to fall in line with the Morbidelli and Gladman (1998) results. We leave an investigation of the collisional evolution of small NEOs to future work.

Our collisional lifetimes for $D > 1$ km objects are higher than those of Farinella *et al.* (1998). For example, we predict that $D \sim 30$ km asteroids have a collisional lifetime of ~ 8 Gy, 4 times longer than Farinella *et al.* (1998). If true, it would insinuate that relatively few such bodies have

---

though we caution that additional work on this topic is needed.

ever disrupted in the main belt. At present, there is no easy way to constrain those values except using the $D > 100$ km asteroids that ended up as prominent families. Still, an analysis of spin vectors among $20 < D < 40$ km asteroids in the Koronis family suggests our CoDDEM collisional lifetimes in this size range may be valid. Slivan (2002) (see also Slivan et al. 2003) found that of the 10 Koronis family members he observed, 4 had prograde spins with nearly identical obliquities (42°-50°) and spin periods (7.5-9.5 h), while the remaining 6 with retrograde spins had obliquities between 154°-169° and spin periods less than 5 hours or greater than 13 hours. Vokrouhlický et al. (2003) demonstrated this unusual configuration was produced by YORP thermal torques (Rubincam 2000; see also Vokrouhlický and Čapek 2002) working on the bodies over 2-3 Gy. Their results imply that the only plausible way these objects could have attained their present rotation states was to avoid major collision events over this time interval. This argues for collisional lifetimes significantly longer than 2-3 Gy, values that would be consistent with our values from CoDDEM.

Overall, our results are comparable (within a factor of $\sim$ 2-10) with recent estimates by Cheng (2004) and O'Brien and Greenberg (2005). The differences are a by-product of different assumptions about the nature and evolution of the main belt size distribution and the use of different Q_D^* functions.

Fig. 15 shows the time interval between catastrophic disruption events across the present-day main belt. The black dots are the intervals for asteroids in each incremental size bin, while the solid line is the interval for objects larger than a given diameter. Using the intervals measured per size bin, we find that a $D \sim 100$ m body disrupts every year in the main belt, while a $D \sim 10$ m body disrupts every day and a $D \sim 1$ m body disrupts about every hour.

EDITOR: PLACE FIGURE 15 HERE.

The Karin cluster is a small asteroid family produced by the disruption of a $D \sim 30$ km parent body 5.8 Ma (Nesvorný et al. 2002b; Nesvorný and Bottke 2004). It is responsible for one of the prominent dust bands observed by IRAS (Nesvorný et al. 2002b; 2003). We predict that $D \sim 30$ km disruption events occur once every 20-25 My across the main belt (see also B05). This timescale seems reasonable to us, given that no other Karin-sized family is producing a prominent dust band detectable by IRAS. If the interval between Karin-size disruption events were only a few My, it is probable that IRAS would have detected several additional dust bands comparable to Karin's band.

On the other hand, we predict that the $D = 170$ km asteroid disruption event that formed the Veritas family 8.3 Ma (Nesvorný et al. 2003) should only occur once per 0.5-1.0 Gy. This implies that (i) the breakup of the Veritas parent body was a statistical fluke, (ii) there are interlopers in the Veritas family and/or the diameters of the family members are poorly characterized, such that its actual parent body was smaller than $D = 170$ km, or (iii) our estimated disruption rates are erroneous and large family-forming events occur more frequently that predicted. While we cannot

rule out (iii), we believe that a significantly higher rate of large- scale disruption events would leave behind an abundance of easily-detected asteroid families in the main belt. For this reason, we believe (i) and/or (ii) provide a more likely explanation for the young age of the Veritas family.

5.3. Constraints from (4) Vesta

Using the methods described in B05, we can determine whether our model size distributions from Table 1 are also consistent with the constraints provided by asteroid (4) Vesta. Recall that Vesta is a $D = 529 \pm 10$ km asteroid with an intact basaltic crust and a singular 460 km diameter crater on its surface (Thomas *et al.* 1997). The fact that Vesta does not have two such remarkable craters can be used to constrain our results. Our test procedure is as follows.

The impactor that created Vesta's crater was $D_{\mathrm{proj}} \sim 35$ km (Marzari *et al.* 1996; Thomas *et al.* 1997; Asphaug 1997). We estimate the average interval between such impacts on Vesta to be:

$$\frac{1}{\tau_{\mathrm{impact}}} = \frac{P_i}{4}(D_{\mathrm{Vesta}} + D_{\mathrm{proj}})^2 \, N(31 \lesssim D \lesssim 39 \text{ km}) \tag{10}$$

where N is the number of available impactors in N_{rem} and N_{dep}. For P_i, we use Vesta's current intrinsic collision probability ($P_i = 2.8 \times 10^{-18}$ km^{-2} yr^{-1}; Farinella and Davis 1992; Bottke *et al.* 1994a). While Fig. 6 and 7 indicate that P_i values for bodies striking N_{rem} do vary over time, we believe our chosen values do a reasonable job of splitting the difference between these changes. To estimate the approximate number of $D \sim 35$ km bodies available in our model runs, we interpolated between the central values of bins $D = 31$ and 39 km in both N_{rem} and N_{dep} at every timestep. We then integrated Eq. (10) across the trial cases from the Table 1 runs that satisfied our constraints. To account for the stochastic nature of the impacts, our model used Poisson statistics and reran our trials 10 times for each run.

We found a reasonable match between our model predictions and data, with the mean number of $D \sim 35$ km objects striking Vesta over 4.6 Gy being 0.5 ± 0.7. This suggests the odds are slightly against Vesta having a single large crater but very much against it having two such craters. While small number statistics prevents us from saying too much about this value, it does appear that our best-fit CoDDEM models can pass a nominal reality check.

5.4. Interpreting the shape and nature of the NEO population

Because our best-fit CoDDEM runs give us insight into the shape of the main belt population, we can use our results to interpret the shape and nature of the NEO population between a few cm and $D \sim 10$ km. Fig. 16 shows the model main belt and NEO populations produced for a representative run from Table 1 where $t_{\mathrm{Jup}} = 3$ My, $f = 180$, $D_x = 110$ km, and Q_{D}^* function #10.

The snapshot of the main belt and NEO populations was taken at 4.6 Gy (i.e., the present day). For reference, we plot our results against an estimate of the NEO population made by Stokes *et al.* (2003), who for simplicity assumed the $D < 1$ km size distribution was a power-law extension of the $D > 1$ km size distribution.

EDITOR: PLACE FIGURE 16 HERE.

Overall, the NEO size distribution is a near reflection of the main belt's wavy-shaped size distribution, with asteroids across the main belt driven to resonances by the Yarkovsky effect (Fig. 1). This mirror-like image is only modestly seen for $D > 1$ km, where the bump near $D \sim 5$ km is damped somewhat in the NEO population relative to the main belt by a steadily decreasing Yarkovsky depletion function. For smaller asteroids, however, the curves near $D \sim 0.2$-0.7 km are prominently seen in both the main belt and NEO populations. Note that this bend is not a by-product of our Yarkovsky removal rate function, which we assume is constant for $D < 1$ km asteroids.

The NEO population at small sizes is constrained, in part, by estimates from telescopic surveys, particularly those from the LINEAR survey (Stuart 2001; D'Abramo *et al.* 2001; Harris 2002; Stuart and Binzel 2004). The size distribution results from LINEAR are based on a larger database than those from Spacewatch and NEAT survey data (Rabinowitz *et al.* 2000), so they are more likely to represent the true NEO population. Constraints also come from estimates of the 1-10 m NEO population derived from satellite detections of bolide detonations in Earth's atmosphere (Brown *et al.* 2002). By assuming that these impactors have the same orbital distribution and intrinsic collision probabilities with Earth as standard NEOs (e.g., Bottke *et al.* 2002b), Brown *et al.* (2002) converted this data into a predicted size distribution. Interestingly, an extension of a line through these constraints also does a good job of fitting the available fireball data (Halliday *et al.* 1996). We caution, however, that the orbital distribution of $D \lesssim 10$ cm particles is essentially unknown, while Poynting-Robertson drag and collisions within the NEO population become increasingly important in this size range.

Given the similarities between the shape of our model main belt, the NEO constraints described above, and our NEO model, we infer that most observed NEOs are of main belt origin. Unless comets have a remarkable similar size distribution, it is likely that they do not contribute significantly to the overall NEO population with $a < 7.4$ AU (e.g., Bottke *et al.* 2002b; Stokes *et al.* 2003).

At face value, the NEO model population shown here is inconsistent with the upper limit value of ~ 10-20 MT airblasts in our atmosphere based on data from the singular 1908 Tunguska event (Morrison *et al.* 2002; Stokes *et al.* 2003). The constraints from LINEAR in the size range are provided by Harris (2002). There are several possible explanations for this inconsistency. The Tunguska blast may have been a statistical fluke (e.g., Morrison *et al.* 2002), or the blast energy may have been poorly characterized (e.g., Appendix 4 of Stokes et al. 2003; see also Edwards *et*

al. 2004). A lower energy would imply a smaller projectile, which would be more in line with our predictions. If not, it is possible that the population of Tunguska-sized impactors has a different orbital distribution than that predicted for km-sized NEOs. More work on this issue is needed.

Assuming our model NEO population is realistic, we find it has approximately 1×10^{10}, 4.5×10^7 14,000, and 1100 asteroids with $D \geq 0.001, 0.01, 0.1$, and 1 km, respectively. Using values from Bottke *et al.* (2002b), we estimate that 67% of all NEOs are on Earth-crossing orbits. If the collision rate of Earth-crossers with Earth is 2.8×10^{-9} yr^{-1}, the interval between km-sized impacts is ~ 0.5 My, in line with previous predictions.

5.5.   Small craters on the terrestrial planets: primaries or secondaries?

Because our model results indicate the main belt population has been relatively constant over the last 3 Gy, we can infer that the NEO model, as well as the impactor flux on the terrestrial planets, has been similarly stable over the same time period. If true, we should be able to directly compare our NEO model population to craters formed on the terrestrial planets over the last 3 Gy.

The most recent investigation of large crater production on the Earth and Moon was by Stuart and Binzel (2004) (see also Morbidelli *et al.* 2002). Using an NEO population determined using debiased LINEAR data, they computed crater production curves that were consistent (within a factor of 2 or so) with $D > 1$ km craters on the lunar maria and $D > 20$ km craters on the Earth. Given that our NEO model population is consistent with Stuart and Binzel (2004), we do not investigate large crater production further in this paper.

For smaller NEOs, our model population could help resolve a long-standing controversy about whether the majority of small craters ($D < 0.1$-1 km) formed on Mercury, the Moon, and Mars were produced by primary impacts or by secondary impacts generated by ejecta from large craters (e.g., Shoemaker 1965). Recent investigations of the surfaces of Mars and Europa provide persuasive evidence that many, perhaps most small craters on these surfaces are secondaries. For example, the rayed Zunil crater on Mars ($D = 10$ km) is believed to have produced $\sim 10^7$ secondary craters > 10 m in diameter within 800 km of the impact site and numerous secondaries in the rays that were within 1600 km of the impact site (McEwen *et al.* 2005). Similarly, more than 95% of the small craters observed on Europa appear to be clustered secondaries derived from large impact structures (Bierhaus *et al.* 2005). When measured in a size distribution, the differential power law slopes of these secondaries are very steep; values of ~ -5 are common, and in certain regions the slopes get as high as -6.5. Overall, the small crater statistics resemble the predictions made for $D < 1$ km craters by standard lunar and martian crater production functions (-4.8 to -5.1; see review by Ivanov *et al.* 2002). The question is whether the slopes of crater size distributions produced by small NEOs are steeper, similar, or shallower than those produced by secondaries. If the answer is shallower, secondaries should dominate the production of small craters on Mercury, the Moon, and Mars.

Terrestrial planet craters are typically 10-20 times larger than the projectile (e.g., Melosh 1989), Thus, to compare our model results with $D < 1$ km craters, we need to transform our $D \lesssim 0.1$ km NEOs into craters. To simplify the problem, we focus on converting the power law slope of our $D < 0.1$ km NEOs into a crater size distribution slope.

Scaling relationships derived by Schmidt and Housen (1987) indicate that $D_{\mathrm{crater}} \propto D_{\mathrm{proj}}^{\gamma}$, where D_{crater} is the crater diameter, D_{proj} is the projectile diameter, and γ is an experimentally-determined parameter that mainly depends on the porosity of the target material. Substituting this relationship into a *differential* power law size distribution, we find that:

$$\alpha_{\mathrm{crat}} = \frac{\alpha_{\mathrm{proj}} + 1}{\gamma} - 1 \tag{11}$$

where α_{proj} is the differential power law index of the projectile population, and α_{crat} is the differential power law index of the crater population.

Schmidt and Housen (1987) estimated that a target surface made of competent rock should have $\gamma = 0.78$. Because our small NEOs have $\alpha_{\mathrm{proj}} = -3.6$, we find $\alpha_{\mathrm{crat}} = -4.3$, a value 0.5-0.8 shallower than the slope values for lunar and martian craters ($\alpha_{\mathrm{crat}} = -4.8$ to -5.1; Ivanov *et al.* 2002). For impacts into hard rock, regolith, soft rock, or dry soil, γ values range between 0.83-0.97 (Holsapple and Housen 2004), which in turn yield even shallower α_{crat} values (-3.7 to -4.1). Recent work in this field also suggests future crater scaling relationships will tend to favor higher γ values (K. Holsapple; personal communication). Regardless, based on these results, we conclude that relatively few of the observed small craters on Mercury, the Moon, and Mars were formed by primary impacts.

Our NEO model differs from crater-based predictions of the NEO population from Werner *et al.* (2001) and Ivanov *et al.* (2002). These groups attempted to use standard crater production functions and crater-scaling relationships (with $\gamma = 0.78$) to determine the nature of the NEO population. An examination of their results, however, suggests they cannot simultaneously reproduce the NEO size distribution for $D \gtrsim 1$ km and $D \lesssim 1$ km. For example, the crater-derived NEO population estimated by Werner *et al.* (2001) is reasonable for large NEOs but does not fit the $D < 0.5$ km data. Ivanov *et al.* (2002) display similar results, though they do show a case where they can match the $D < 0.01$ km data at the cost of missing the $D > 0.1$ km data. While some of these mismatches may stem from poorly-known crater- scaling relationships, we believe the main factor is that the crater size distributions on Mercury, Mars, and Moon are dominated by secondaries at small crater sizes.

In conclusion, we believe extreme caution should be used when dating surfaces using $D < 0.1$-1 km craters. New work will be needed to determine whether the projectile population described here can be used to infer the ages of such surfaces.

5.6. Evidence for early asteroid disruption events from meteorites

Ideally, meteorites can be used to help constrain the number and nature of catastrophic disruption events in the primordial main belt. As discussed below, however, this record does not easily yield its secrets about what took place 4.4-4.6 Gy ago.

To probe for early collision events, many meteoriticists examine radiometric or isotopic reset ages. These ages can be used to tell us when the meteorite parent body was formed in the Solar Nebula, when it crystallized from an igneous melt, or when it was altered by a heating event. The heating events germane to our purposes are those produced by impacts. In some cases, impact-induced shock degassing events can be used to infer impact and reassembly events on meteorite parent bodies. The chronometers used for these studies are based on common parent-daughter isotopic pairs, such as: ^{40}K-^{40}Ar, ^{87}Rb-^{87}Sr, ^{147}Sm- ^{143}Nd, ^{235}U-^{207}Pb, and ^{238}U-^{206}Pb (Mittlefehldt *et al.* 1998).

The problem with shock degassing ages is they typically only record the last resetting event that occurred on the meteorite's immediate precursor. For example, multiple resetting events detected on meteorites from the HED parent body, the mesosiderite parent body, and L, LL, and H ordinary chondrite parent bodies occurred $\sim$ 3.9 Ga (Bogard 1995), the same time that the LHB took place on the Moon (e.g., Hartmann *et al.* 2000). Impacts produced by projectiles over the last 3.9 Gy appear to have obscured or erased radiometric age evidence for asteroid-asteroid impacts that occurred $\gtrsim$ 3.9 Gyr. Thus, if we want to probe deeper into the earliest days of main belt history, we need to turn to other meteoritical clues.

It turns out that for 7 groups of meteorites, there is textural and cooling rate evidence that their parent bodies were shattered and reassembled early in solar system history (e.g., Mittlefehldt *et al.* 1998). Available data supports a scenario where hot interior material, presumably heated by the decay of ^{26}Al or the decay of some other short-lived radiogenic isotope, was suddenly mixed with cool material near the surface. These parent bodies include those for the Shallowater enstitite achondrites, the mesosiderites, the H and L chondrites, the ureilite achondrites, the IVA irons, and the parent body of the IAB irons and winonaites (Keil *et al.* 1994; Benedix *et al.* 2000; Scott *et al.* 2001; see reviews in Mittlefehldt *et al.* 1998; Scott 2002; and Haack and McCoy 2004). Details on these events are given below:

- The H ordinary chondrite parent body, thought to have a parent body diameter $D_{pb} \lesssim 200$ km, appears to have gone through some degree of impact scrambling > 4.4 Ga ago (Keil *et al.* 1994). Apparently, this event was not thorough enough to disturb the cooling rates of some H chondrites (Trieloff *et al.* 2003; Scott *et al.* 2003). Grains taken from L chondrite impact breccias, where $D_{pb} > 100$ km, also yield impact scrambling ages of > 4.4 Ga (Keil *et al.* 1994).

- The mesosiderite parent body, thought to be $200 < D_{pb} < 400$ km, appears to have been differentiated prior to its impact scrambling event. Scott *et al.* (2001) argue that the

silicate and metallic breccias observed in the mesosiderites were likely produced when the mesosiderite parent body was struck by a $50 < D < 150$ km projectile ~ 4.4-4.45 Ga.

- There are 26 IAB irons containing silicate-bearing inclusions called winonaites. Collectively, these meteorites yield formation ages of 4.4-4.54 Ga (Benedix *et al.* 2000). Studies suggest that the partially differentiated IAB iron-winonaite parent body, thought to be $20 < D_{pb} < 60$ km, was impact scrambled and reassembled, allowing the silicates to mix with molten iron from the core.

- The ureilite achondrites are coarse-grained rocks made predominately of olivine and pyroxene; it is believed they formed within a single asteroid 4.55 Ga. (e.g., Goodrich 1992; Torigoye-Kita *et al.* 1995). Their parent body, thought to be $D_{pb} > 200$ km (Goodrich *et al.* 2002), was scrambled and reassembled ~ 4.5 Ga, with the ureilites dramatically cooled at rates of 3-20° h^{-1} (Mori and Takeda 1983).

- Studies of the Shallowater enstatite chondrite, an unbrecciated igneous aubrite, indicate they were produced by a shattering collision on the molten or partly-molten enstatite parent body ~ 4.5 Ga (Keil *et al.* 1989). Their cooling history, however, is complicated; in one scenario, these meteorites: (i) cooled rapidly by exposure to space via an impact, (ii) were buried by the reassembly of the shattered parent body (i.e., at depths of 40 km on a $D_{pb} = 100$ km parent body), and (iii) were later reburied by a second impact that moved this material near the parent body's surface.

We point out that the interpretation of these records requires considerable care, and that the above scenarios are not universally accepted by the meteorite community. Nevertheless, the weight of evidence suggests that some large asteroids with hot interiors experienced significant shattering/reassembly events > 4.4 Ga. At the least, these results imply that the main belt was undergoing fragmentation very early in its history. We also find it interesting that the timescale of these events is consistent with our model predictions, though one must be cautious not to over- interpret the data. Recall that the interiors of $D \gtrsim 100$ km parent bodies cool fast enough that shattering/reassembly events occurring < 4.4 Ga may not leave behind obvious meteoritical signatures (e.g., McSween *et al.* 2002). Thus, the paucity of textural and cooling rate evidence for < 4.4 Gy impact events does not necessarily imply a dramatic change in the collision rate.

6. Conclusions

Here we summarize the main conclusions of this paper.

It has long been known that the main belt zone is significantly depleted in mass compared to expectations from standard solar nebula estimates (i.e., $5 \times 10^{-4} M_\oplus$ vs. $\sim M_\oplus$, respectively). The best available dynamical model to explain this mass loss (Petit *et al.* 2001) suggests that the post-accretion main belt went through three broad phases of evolution:

Phase 1. An early phase lasting a few My where planetesimals and planetary embryos both accreted and dynamical excited one another enough to initiate fragmentation. Gravitational perturbations from newly-grown planetary embryos both inside and outside the primordial main belt combined to dynamically stir the population, enough to pump up e and i values and increase collision velocities. At this point, accretion ended and fragmentation began. The population was large enough that collisional evolution occurred quickly, though not so quickly as to remove a significant portion of the overall mass. Collisions disrupted many bodies, some which were likely differentiated. All disruption events produced significant numbers of fragments, enough that the main belt size distribution began to take on a wavy shape similar to that observed in the current main belt. Hence, B05 characterized this shape as a "fossil" left over from this early violent epoch.

Phase 2. A second phase initiated by the accretion of Jupiter's gaseous envelope that may lasted as long as several hundreds of My. In this phase, gravitational perturbations between Jupiter and planetary embryos dynamically eject more than 99% of the bodies out of the main belt zone. Collisions between this newly excited population and the main belt survivors produce numerous disruption events, though dynamical processes quickly eliminate most bodies from the excited population. In the process, all dynamical evidence for asteroid families prior to the dynamical excitation event is lost. Although the objects left behind are unlikely to have any dynamical association with one another, the semimajor axis spreading produced by this event only moderately modifies the radial spread of the S-, C-, and P- type asteroids. Meteoritical evidence for comminution during Phases 1 and 2 is reviewed in Sec. 5.6.

Phase 3. The third phase begins when the ejected main belt population is no longer significant enough to produce meaningful numbers of disruption events among the surviving main belt population. Nominally, this time span lasts from several hundred My after the formation of the solar system to the present day. In this phase, the surviving main belt population is only modestly different from the observed population. Collision events are relatively rare and occur at the frequency estimated by B05. Note that we our model does not account for the (unknown) effects of the Late Heavy Bombardment (see Sec. 2.2.4).

Using our collisional and dynamical depletion evolution model CoDDEM, we tracked the evolution of the main belt from the end of planetary accretion and the onset of fragmentation to the present. This code accounts for catastrophic disruption events, asteroid fragmentation, and the excitation and loss of material via the dynamical processes described in Phase 2. CoDDEM's

results were constrained by the main belt's size-frequency distribution, the number of asteroid families produced by $D > 100$ km disruptions over the last 3.5 Gy, the presence of a single large impact crater on Vesta's intact basaltic crust, and the constant lunar and terrestrial impactor flux (within a factor of 2) over the last 3 Gy.

We used CoDDEM to test the effects of particular variables, including the disruption scale law Q_D^* (Fig. 5), the initial main belt size distribution (D_x; see Fig. 9), the magnitude of the primordial population f in $D < 1000$ km bodies, where $f = 1$ is the current main belt's mass, and the formation time of Jupiter $t_{\rm Jup}$.

Our best fit results indicate that the primordial main belt (for planetesimals with $D \lesssim 1000$ km) once had a differential power law slope for $D \gtrsim 110$ km asteroids of -4.5, the same slope found in the main belt today. Tests indicate the slope for $D \lesssim 110$ km was shallow (e.g., Sec. 4.1). The Q_D^* function providing the greatest number of model fits to our constraints was #10 of Fig. 5. This function is only slightly shallower in the gravity regime than the Q_D^* function computed using the SPH calculations of Benz and Asphaug (1999). Interestingly, these results appear to be consistent with recent numerical impact experiments where pre-shattered target bodies were substituted for undamaged ones (P. Michel, personal communication).

The best fit cases from our production runs (Fig. 12) are given in Table 1 (see Sec. 4.3). They suggest that f, the number of current main belt masses in the initial main belt population, and $t_{\rm Jup}$, the time of Jupiter's formation relative to the onset of fragmentation in the main belt, are coupled, with a best-fit envelope of values yielding $f = 186$ My $- 8.2 \, t_{\rm Jup}$. The mean and median $t_{\rm Jup}$ values are 3.3 ± 2.6 My and 2 My, respectively. Though our model suggests that Jupiter could have formed at nearly any time between 1-10 My, the most likely formation time is $t_{\rm Jup} \leq 4$ My. These results agree with the estimated mean disk lifetime of 3 My predicted by Haisch *et al.* (2001). The mean and median values of f are 160 ± 44 and 150, respectively. This corresponds to 0.06-$0.1 M_\oplus$, a small fraction of the total mass that is thought to have once existed in the main belt zone during planet formation (Weidenschilling 1977). The remainder was likely to have been contained in planetary embryos. These results agree with dynamical results from Petit *et al.* (2001), who found that $\sim 0.5\%$ of the test bodies initially emplaced in the primordial main belt would survive the DDE. They also are consistent with back-of-the-envelope calculations made by B05.

We predict that numerous $D > 200$ km bodies disrupted in the $N_{\rm dep}$ population (i.e., the fraction of the main belt dynamically depleted in Phase 2) during Phases 1 and 2, with a small fraction of their fragments reaching the safety of the main belt zone (Sec. 5.1). Survivors from these disrupted and dispersed differentiated objects could produce several different asteroid taxonomic types: iron-rich asteroids from the core might be analogous to some M-type asteroids, olivine-rich metal-free silicate asteroids from the mantle might be analogous to A-type asteroids, and basalt-rich asteroids from the crust might be analogous to V-type asteroids. More specifically, these fragments may explain the presence of (1459) Magnya, a $D = 30$ km V-type asteroid located

in the outer main belt (Lazzaro *et al.* 2000; Michtchenko *et al.* 2002), (16) Psyche and (216) Kleopatra, M-type asteroids with pulverized iron-like radar albedos (Magri *et al.* 1999; 2001; see also Davis *et al.* 1999), and several observed olivine-rich A-type asteroids (Xu *et al.* 1995; Bus and Binzel 2002a,b).

Our collisional lifetimes agree with the estimated lifetime of fireballs, the CRE ages of stony meteorites, and the production rate of asteroid families from $D > 100$ km breakup events (Sec. 5.2). They also agree with the inferred degree of collisional activity in the Koronis family over the last several Gy (Vokrouhlický *et al.* 2003). Our results indicate that main belt asteroids with $D = 0.001, 0.01, 0.1, 1, 10,$ and 100 km have an average collisional lifetime of 14, 27, 64, 440, 4,700, and 34,000 My, respectively. For the largest asteroids, these results imply that relatively few have disrupted over the last several Gy. As discussed in B05, the available evidence suggests that most $D > 110$ km asteroids are primordial while many/most $D < 110$ km asteroids are fragments (see also B05). Our best fit results are also consistent with the production of a single $D = 460$ km crater on (4) Vesta (Sec. 5.3).

In Sec. 5.4, we discussed how our model allows us to interpret the shape and nature of the NEO population, which is constrained by observations from LINEAR (Stuart 2001; D'Abramo *et al.* 2001; Harris 2002; Stuart and Binzel 2004), satellite detections of bolide detonations in Earth's atmosphere (Brown *et al.* 2002), and observed fireball data (Halliday *et al.* 1996). Using a simple Yarkovsky loss rate function, we showed that the shape of the NEO size distribution is primarily a reflection of the main belt's size distribution. Our model indicates the current NEO population has been in steady state for the last 3 Gy, results which are consistent with impact rates derived for the Earth and Moon.

Using our NEO model, we explored in Sec. 5.5 whether the majority of small craters ($D < 0.1$-1 km) on Mercury, the Moon, and Mars were produced by primary impacts or by secondary impacts generated by ejecta from large craters. Using data from laboratory experiments and explosion craters (Schmidt and Housen 1987; Holsapple and Housen 2004) and our model results, we determined that primary craters formed by $D \lesssim 0.1$ km projectiles should produce a differential power law slope of -4.3 or shallower. This value is 0.5-0.8 shallower than the differential slope values estimated from lunar and martian craters (-4.8 to -5.1; Ivanov *et al.* 2002). Other crater scaling relationships imply the slope difference could be even larger. Based on these results, we believe that most small craters on Mercury, the Moon, and Mars are secondaries.

Acknowledgements

REFERENCES

Agnor, C. B., Canup, R. M., Levison, H. F. 1999. On the Character and Consequences of Large Impacts in the Late Stage of Terrestrial Planet Formation. Icarus 142, 219-237.

Agnor, C., Asphaug, E. 2004. Accretion Efficiency during Planetary Collisions. Astrophysical Journal 613, L157-L160.

Alibert, Y., Mordasini, C., Benz, W. 2004. Migration and giant planet formation. Astronomy and Astrophysics 417, L25-L28.

Asphaug, E. 1997. Impact origin of the Vesta family. Meteoritics and Planetary Science 32, 965-980.

Asphaug, E., Agnor, C., Williams, Q. 2005. Tidal Forces as Drivers of Collisional Evolution. 36th Annual Lunar and Planetary Science Conference 36, 2393.

Bendjoya, P., Zappalà, V. 2002. Asteroid Family Identification. In *Asteroids III* (Eds. W.F. Bottke, A. Cellino, P. Paolicchi, and R.P. Binzel), Univ. of Arizona Press, Tucson, 613-618.

Benedix, G. K., McCoy, T. J., Keil, K., Love, S. G. 2000. A petrologic study of the IAB iron meteorites: Constraints on the formation of the IAB-Winonaite parent body. Meteoritics and Planetary Science 35, 1127-1141.

Benz, W. and E. Asphaug 1999. Catastrophic Disruptions Revisited. Icarus 142, 5-20.

Bierhaus, E. B., C. R. Chapman, and W. J. Merline. 2005. Secondary craters on Europa and implications for cratered surfaces. Nature, in press.

Bogard, D. 1995. Impact ages of meteorites: A synthesis. Meteoritics 30, 244-268.

Bottke, W. F., Greenberg, R. 1993. Asteroidal collision probabilities. Geophysical Research Letters 20, 879-881.

Bottke, W.F., M.C. Nolan, R. Greenberg, and R.A. Kolvoord. 1994a. Velocity Distributions among Colliding Asteroids. Icarus 107, 255–268.

Bottke, W. F., M. C. Nolan, R. Greenberg, and R. A. Kolvoord. 1994b. Collisional lifetimes and impact statistics of near-Earth asteroids. In *Hazards Due to Comets and Asteroids* (Eds, T. Gehrels, M. S. Matthews) Univ. of Arizona Press, Tucson, 337–357.

Bottke, W. F., R. Jedicke, A. Morbidelli, J. -. Petit and B. Gladman 2000. Understanding the Distribution of Near-Earth Asteroids. Science 288, 2190-2194

Bottke, W.F. Jr., D.P. Rubincam, and J.A. Burns 2000a. Dynamical Evolution of Main Belt Meteoroids: Numerical Simulations Incorporating Planetary Perturbations and Yarkovsky Thermal Forces. Icarus 145, 301–331.

Bottke, W. F., D. Vokrouhlický, M. Brož, D. Nesvorný, and A. Morbidelli 2001. Dynamical Spreading of Asteroid Families by the Yarkovsky Effect. Science 294, 1693-1696.

Bottke, W. F., D. Vokrouhlický, D. Rubincam, and M. Brož, 2002b. Dynamical Evolution of Asteroids and Meteoroids using the Yarkovsky Effect. In *Asteroids III* (Eds. W.F. Bottke, A. Cellino, P. Paolicchi, and R.P. Binzel), Univ. of Arizona Press, Tucson, 395-408.

Bottke, W. F., A. Morbidelli, R. Jedicke, J. Petit, H. F. Levison, P. Michel, and T. S. Metcalfe 2002b. Debiased Orbital and Absolute Magnitude Distribution of the Near-Earth Objects. Icarus 156, 399-433.

Bottke, W. F., D. Durda, D. Nesvorny, R. Jedicke, A. Morbidelli, D. Vokrouhlicky, and H. Levison. 2005. The fossilized size distribution of the main asteroid belt. Icarus 175, 111-140.

Britt, D. T., Yeomans, D., Housen, K., Consolmagno, G. 2002. Asteroid Density, Porosity, and Structure. In *Asteroids III* (Eds. W.F. Bottke, A. Cellino, P. Paolicchi, and R.P. Binzel), Univ. of Arizona Press, Tucson, 485-500.

Brown, P., Spalding, R. E., ReVelle, D. O., Tagliaferri, E., Worden, S. P. 2002. The flux of small near-Earth objects colliding with the Earth. Nature 420, 294-296.

Burbine, T. H., Meibom, A., Binzel, R. P. 1996. Mantle material in the main belt: Battered to bits?. Meteoritics and Planetary Science 31, 607-620.

Burbine, T. H., McCoy, T. J., Meibom, A., Gladman, B., Keil, K. 2002. Meteoritic Parent Bodies: Their Number and Identification. In *Asteroids III* (Eds. W.F. Bottke, A. Cellino, P. Paolicchi, and R.P. Binzel), Univ. of Arizona Press, Tucson, 653-667.

Bus, S. J., Binzel, R. P. 2002a. Phase II of the Small Main-Belt Asteroid Spectroscopic Survey: The Observations. Icarus 158, 106-145.

Bus, S. J., Binzel, R. P. 2002b. Phase II of the Small Main-Belt Asteroid Spectroscopic Survey: A Feature-Based Taxonomy. Icarus 158, 146-177.

Campo Bagatin, A., A. Cellino, D. R. Davis, P. Farinella, and P. Paolicchi 1994. Wavy size distributions for collisional systems with a small-size cutoff. Plan. Space Sci. 42, 1079-1092.

Canup, R. M. 2004. Dynamics of Lunar Formation. Annual Review of Astronomy and Astrophysics 42, 441-475.

Cellino, A., S. J. Bus, A. Doressoundiram, and D. Lazzaro 2002. Spectroscopic Properties of Asteroid Families. In *Asteroids III* (Eds. W.F. Bottke, A. Cellino, P. Paolicchi, and R.P. Binzel), Univ. of Arizona Press, Tucson, 633-643.

Chambers, J. E., Migliorini, F. 1997. Mercury - A New Software Package for Orbital Integrations. Bulletin of the American Astronomical Society 29, 1024.

Chambers, J. E. and G. W. Wetherill 1998. Making the Terrestrial Planets: N-Body Integrations of Planetary Embryos in Three Dimensions. Icarus 136, 304-327.

Chambers, J. E. and G. W. Wetherill 2001. Planets in the asteroid belt. Meteoritics and Planetary Science 36, 381-399.

Chambers, J. E., Cassen, P. 2002. The effects of nebula surface density profile and giant-planet eccentricities on planetary accretion in the inner solar system. Meteoritics and Planetary Science 37, 1523-1540.

Cheng, A. F. 2004. Collisional evolution of the asteroid belt. Icarus 169, 357-372

Colwell, J. E. 1993. Power-Law Confusion: You Say Incremental, I Say Differential. Lunar and Planetary Institute Conference Abstracts 24, 325.

Culler, T. S., T. A. Becker, R. A. Muller, and P. R. Renne. 2000. Lunar impact history from ^{40}Ar/^{39}Ar dating of glass spherules. Science 287, 1785-1788.

D'Abramo, G., Harris, A. W., Boattini, A., Werner, S. C., Harris, A. W., Valsecchi, G. B. 2001. NOTE: A Simple Probabilistic Model to Estimate the Population of near-Earth Asteroids. Icarus 153, 214-217.

Davis, D. R., C. R. Chapman, R. Greenberg, S. J. Weidenschilling, and A. W. Harris 1979. Collisional evolution of asteroids - Populations, rotations, and velocities. In *Asteriods* (Ed. T. Gehrels) Univ. of Arizona Press, Tucson, 528-557.

Davis, D. R., Farinella, P., Marzari, F. 1999. The Missing Psyche Family: Collisionally Eroded or Never Formed? Icarus 137, 140-151.

Davis, D. R., Durda, D. D., F. Marzari, A. Campo Bagatin, and R. Gil-Hutton. 2002. Collisional Evolution of Small Body Populations. In *Asteroids III* (Eds. W.F. Bottke, A. Cellino, P. Paolicchi, and R.P. Binzel), Univ. of Arizona Press, Tucson, 545-558.

Dermott, S. F., Durda, D. D., Grogan, K., Kehoe, T. J. J. 2002. Asteroidal Dust. In *Asteroids III* (Eds. W.F. Bottke, A. Cellino, P. Paolicchi, and R.P. Binzel), Univ. of Arizona Press, Tucson, 423-442.

Dohnanyi, J. W. 1969. Collisional models of asteroids and their debris. J. Geophys. Res. 74, 2531-2554.

Durda, D. D., R. Greenberg, and R. Jedicke 1998. Collisional Models and Scaling Laws: A New Interpretation of the Shape of the Main-Belt Asteroid Size Distribution. Icarus 135, 431-440.

Durda, D. D., Bottke, W. F., Enke, B. L., Merline, W. J., Asphaug, E., Richardson, D. C., Leinhardt, Z. M. 2004. The formation of asteroid satellites in large impacts: results from numerical simulations. Icarus 170, 243-257.

Edwards, W. N., Brown, P. G., ReVelle, D. O. 2004. Bolide Energy Estimates from Measured Infrasonic Signal Properties. AAS/Division for Planetary Sciences Meeting 36, 1150.

Eugster, O. 2003, Cosmic-ray exposure ages of meteorites and lunar rocks and their significance. Chemie der Erde 63, 3-30.

Farinella, P. and D. R. Davis 1992. Collision rates and impact velocities in the Main Asteroid Belt. Icarus 97, 111-123.

Farinella, P., Froeschle, C., Gonczi, R., Hahn, G., Morbidelli, A., Valsecchi, G. B. 1994. Asteroids Falling Into the Sun. Nature 371, 314.

Farinella, P., D. Vokrouhlicky, and W. K. Hartmann 1998. Meteorite Delivery via Yarkovsky Orbital Drift. Icarus 132, 378-387.

Farinella, P. and D. Vokrouhlicky 1999. Semimajor axis mobility of asteroidal fragments. Science 283, 1507-1510

Fowler, J.W. and J.R. Chillemi. 1992. IRAS asteroid data processing. In The IRAS Minor Planet Survey (E.F. Tedesco, ed) Tech. Report PL-TR-92-2049., Phillips Laboratory, Hanscom Air Force Base, Massachusetts, pp 17-43.

Franklin, F., Lecar, M. 2000. On the transport of bodies within and from the asteroid belt. Meteoritics and Planetary Science 35, 331-340.

Gladman, B. J., Migliorini, F., Morbidelli, A., Zappala, V., Michel, P., Cellino, A., Froeschle, C., Levison, H. F., Bailey, M., Duncan, M. 1997. Dynamical lifetimes of objects injected into asteroid belt resonances. Science 277, 197-201.

Goodrich, C. A. 1992. Ureilites - A critical review. Meteoritics 27, 327-352.

Goodrich, C. A., Krot, A. N., Scott, E. R. D., Taylor, G. J., Fioretti, A. M., Keil, K. 2002. Formation and Evolution of the Ureilite Parent Body and Its Offspring. Lunar and Planetary Institute Conference Abstracts 33, 1379.

Gomes, R. S. 1997. Dynamical Effects of Planetary Migration on the Primordial Asteroid Belt. Astronomical Journal 114, 396-401.

Gomes, R., K. Tsiganis, A. Morbidelli, and H. F. Levison. 2004. The late heavy bombardment as a cataclysimic event caused by a delayed planetary migration. Nature, submitted.

Gradie, J., Tedesco, E. 1982. Compositional structure of the asteroid belt. Science 216, 1405-1407.

Grieve, R. A. F., Shoemaker, E. M. 1994. The Record of Past Impacts on Earth. In Hazards Due to Comets and Asteroids (Eds. T. Gehrels, M. S. Matthews) U. Arizona Press. 417-462.

Grimm, R. E., McSween, H. Y. 1993. Heliocentric zoning of the asteroid belt by aluminum-26 heating. Science 259, 653-655.

Grinspoon, D. H. 1989. Large impact events and atmospheric evolution on the terrestrial planets. Ph.D. Thesis.

Greenberg, R. 1982. Orbital interactions - A new geometrical formalism. Astronomical Journal 87, 184-195.

Greenberg, R., W. K. Hartmann, C. R. Chapman, and J. F. Wacker 1978. Planetesimals to planets - Numerical simulation of collisional evolution. Icarus 35, 1-26.

Greenberg, R., Nolan, M. C., Bottke, W. F., Kolvoord, R. A., Veverka, J. 1994. Collisional history of Gaspra. Icarus 107, 84.

Greenberg, R., Bottke, W. F., Nolan, M., Geissler, P., Petit, J., Durda, D. D., Asphaug, E., Head, J. 1996. Collisional and Dynamical History of Ida. Icarus 120, 106-118.

Grier, J. A., McEwen, A. S., Lucey, P. G., Milazzo, M., Strom, R. G. 2001. Optical maturity of ejecta from large rayed lunar craters. Journal of Geophysical Research 106, 32847-32862.

Haack, H. and T. J. McCoy. 2004. Iron and stony iron meteorites. In *Treatise on Geochemistry* (Eds. H. D. Holland and K.K. Turekian), Elsevier-Pergamon, Oxford.

Haisch, K. E., Lada, E. A., Lada, C. J. 2001. Disk Frequencies and Lifetimes in Young Clusters. Astrophysical Journal 553, L153-L156

Halliday, I., Griffin, A. A., Blackwell, A. T. 1996. Detailed data for 259 fireballs from the Canadian camera network and inferences concerning the influx of large meteoroids. Meteoritics and Planetary Science 31, 185-217.

Harris, A. W. 2002. A New Estimate of the Population of Small NEAs. Bulletin of the American Astronomical Society 34, 835.

Hartmann, W. K. 1975. Lunar 'cataclysm' - A misconception. Icarus 24, 181-187.

Hartmann, W. K., R. Strom, S. Weidenschilling, K. Blasius, A. Woronow, M. Dence, R. Grieve, J. Diaz, C. Chapman, E. Shoemaker, and K. Jones (1981) Chronology of Planetary Volcanism by Comparative Studies of Planetary Craters. In "Basaltic Volcanism on the Terrestrial Planets" (Basaltic Volcanism Study Project), pp. 1050-1127. (Elmsford, NY: Pergamon Press).

Hartmann, W. K., Ryder, G., Dones, L., and Grinspoon, D. (2000) The time-dependent intense bombardment of the primoridal Earth/Moon system. In *Origin of the Earth and the Moon* (Eds, R. Canup and K. Righter) Univ. of Arizona Press, Tucson., 805-826.

Hartung, J. B. 1974. Can random impacts cause the observed Ar 39/40 age distribution for lunar highland rocks? Meteoritics 9, 349.

Heppenheimer, T. A. 1980. Secular resonances and the origin of eccentricities of Mars and the asteroids. Icarus 41, 76-88.

Holsapple, K. A., Housen, K. R. 2004. The Cratering Database: Making Code Jockeys Honest. Lunar and Planetary Institute Conference Abstracts 35, 1779.

Hörz, F. 2000. Time-variable cratering rates? Science 288, 2095a.

Hubickyj, O., Bodenheimer, P., Lissauer, J. 2003. Small Core for Jupiter using the Core Instability Model. AAS/Division for Planetary Sciences Meeting 35, Abstract 25.06.

Ida, S., Lin, D. N. C. 1996. Long Term Gas Drag Effect on the Structure of the Asteroid Belt and its Implications for the Solar Nebula. Astronomical Journal 112, 1239.

Inaba, S., G. W. Wetherill, and M. Ikoma 2003. Formation of gas giant planets: core accretion models with fragmentation and planetary envelope. Icarus 166, 46-62.

Ip, W.-H. 1987. Gravitational Stirring of the Asteroid Belt by Jupiter Zone Bodies. Beitraege zur Geophysik 96, 44-51.

Ivanov, B. A., G. Neukum, W. F. Bottke, and W. K. Hartmann. 2002. The comparison of size-frequency distributions of impact craters and asteroids and the planetary cratering rate. In *Asteroids III* (Eds. W.F. Bottke, A. Cellino, P. Paolicchi, and R.P. Binzel), Univ. of Arizona Press, Tucson, 89-101.

Ivezić, Željko and 32 colleagues 2001. Solar System Objects Observed in the Sloan Digital Sky Survey Commissioning Data. Astron. J. 122, 2749-2784

Jedicke, R. and T. S. Metcalfe 1998. The orbital and absolute magnitude distributions of main belt asteroids. Icarus 131, 245-260

Jedicke, R., J. Larsen, and T. Spahr. 2002. Observational selection effects in asteroid surveys. In *Asteroids III* (Eds. W.F. Bottke, A. Cellino, P. Paolicchi, and R.P. Binzel), Univ. of Arizona Press, Tucson, 71-87.

Keil, K. 1989. Enstatite meteorites and their parent bodies. Meteoritics 24, 195-208.

Keil, K. 2002. Geological History of Asteroid 4 Vesta: The "Smallest Terrestrial Planet". In *Asteroids III* (Eds. W.F. Bottke, A. Cellino, P. Paolicchi, and R.P. Binzel), Univ. of Arizona Press, Tucson, 573-584.

Keil, K., Haack, H., Scott, E. R. D. 1994. Catastrophic fragmentation of asteroids: Evidence from meteorites. Planetary and Space Science 42, 1109-1122.

Kokubo, E., Ida, S. 2002. Formation of Protoplanet Systems and Diversity of Planetary Systems. Astrophysical Journal 581, 666-680.

Kortenkamp, S. J. and G. W. Wetherill 2000. Terrestrial Planet and Asteroid Formation in the Presence of Giant Planets. I. Relative Velocities of Planetesimals Subject to Jupiter and Saturn Perturbations. Icarus 143, 60-73.

Kortenkamp, S. J., G. W. Wetherill, S. Inaba, and D. E. Trilling 2001. Asteroid Formation with a Pre-Existing Jupiter. Lunar and Planetary Institute Conference Abstracts 32, 1796.

Knežević, Z., Lemaître, A., Milani, A. 2002. The Determination of Asteroid Proper Elements. In *Asteroids III* (Eds. W.F. Bottke, A. Cellino, P. Paolicchi, and R.P. Binzel), Univ. of Arizona Press, Tucson, 603-612.

Kuzmanoski, M., Kovačević, A. 2002. Motion of the asteroid (13206) 1997GC22 and the mass of (16) Psyche. Astronomy and Astrophysics 395, L17-L19.

Lazzaro, D., Michtchenko, T., Carvano, J. M., Binzel, R. P., Bus, S. J., Burbine, T. H., Mothé-Diniz, T., Florczak, M., Angeli, C. A., Harris, A. W. 2000. Discovery of a Basaltic Asteroid in the Outer Main Belt. Science 288, 2033-2035.

Levison, H. F., Dones, L., Chapman, C. R., Stern, S. A., Duncan, M. J., and Zahnle, K. 2001. Could the Lunar "Late Heavy Bombardment" have been triggered by the formation of Uranus and Neptune? Icarus, 151, 286-306

Levison, H. F., Stewart, G. R. 2001. Remarks on Modeling the Formation of Uranus and Neptune. Icarus 153, 224-228

Liou, J. C., Malhotra, R. 1997. Depletion of the outer asteroid belt. Science 275, 375-377.

Lissauer, J. J. 1987. Timescales for planetary accretion and the structure of the protoplanetary disk. Icarus 69, 249-265.

Magri, C., Ostro, S. J., Rosema, K. D., Thomas, M. L., Mitchell, D. L., Campbell, D. B., Chandler, J. F., Shapiro, I. I., Giorgini, J. D., Yeomans, D. K. 1999. Mainbelt Asteroids: Results of Arecibo and Goldstone Radar Observations of 37 Objects during 1980-1995. Icarus 140, 379-407.

Magri, C., Consolmagno, G. J., Ostro, S. J., Benner, L. A. M., Beeney, B. R. 2001. Radar constraints on asteroid regolith compositions using 433 Eros as ground truth. Meteoritics and Planetary Science 36, 1697-1709.

Marti, K., Graf, T. 1992. Cosmic-ray exposure history of ordinary chondrites. Annual Review of Earth and Planetary Sciences 20, 221-243.

Marzari, F., A. Cellino, D. R. Davis, P. Farinella, V. Zappalà, and V. Vanzani 1996. Origin and evolution of the Vesta asteroid family. Astronomy and Astrophysics 316, 248-262.

Marzari, F., Farinella, P., Davis, D. R. 1999. Origin, Aging, and Death of Asteroid Families. Icarus 142, 63-77.

McEwen, A. S., Moore, J. M., Shoemaker, E. M. 1997. The Phanerozoic impact cratering rate: Evidence from the farside of the Moon. Journal of Geophysical Research 102, 9231-9242.

McEwen, A. S., B. S. Preblich, E. P. Turtle, N. A. Artemieva, M. P. Golombek, M.Hurst, R. L. Kirk, D. M. Burr, and P. R. Christensen. 2005. The rayed crater Zunil and interpretation s of small impact craters on Mars, Icarus, in press.

McNeil, D. S., Duncan, M. J., Levison, H. F. 2004. Effects of Type I Migration on Terrestrial Planet Formation. AAS/Division for Planetary Sciences Meeting Abstracts 36, 1177.

McSween, H. Y., Ghosh, A., Grimm, R. E., Wilson, L., Young, E. D. 2002. Thermal Evolution Models of Asteroids. In *Asteroids III* (Eds. W.F. Bottke, A. Cellino, P. Paolicchi, and R.P. Binzel), Univ. of Arizona Press, Tucson, 559-571.

Melosh, H. J. 1989. Impact cratering: A geologic process. Oxford University Press (Oxford Monographs on Geology and Geophysics, No. 11), 1989, 253.

Milani, A., Knežević, Z. 1994. Asteroid proper elements and the dynamical structure of the asteroid main belt. Icarus 107, 219-254.

Michtchenko, T. A., Lazzaro, D., Ferraz-Mello, S., Roig, F. 2002. Origin of the Basaltic Asteroid 1459 Magnya: A Dynamical and Mineralogical Study of the Outer Main Belt. Icarus 158, 343-359.

Mittlefehldt D.W., McCoy T.J., Goodrich C.A. and Kracher A. 1998. Non-chondritic meteorites from asteroidal bodies. In *Planetary Materials* (Ed., J.J. Papike), Reviews in Mineralogy 36, 4-1-4-195.

Morbidelli, A. and B. Gladman 1998. Orbital and temporal distributions of meteorites originating in the asteroid belt. Meteoritics and Planetary Science 33, 999-1016

Morbidelli, A., J. Chambers, J. I. Lunine, J. M. Petit, F. Robert, G. B. Valsecchi, and K. E. Cyr 2000. Source regions and time scales for the delivery of water to Earth. Meteoritics and Planetary Science 35, 1309-1320.

Morbidelli, A., Petit, J.-M., Gladman, B., Chambers, J. 2001. A plausible cause of the late heavy bombardment. Meteoritics and Planetary Science 36, 371-380.

Morbidelli, A., Jedicke, R., Bottke, W. F., Michel, P., Tedesco, E. F. 2002. From Magnitudes to Diameters: The Albedo Distribution of Near Earth Objects and the Earth Collision Hazard. Icarus 158, 329-342.

Morbidelli, A. and D. Vokrouhlický 2003. The Yarkovsky-driven origin of near-Earth asteroids. Icarus 163, 120-134.

Mori, H., Takeda, H. 1983. An Electron Petrographic Study of Ureilite Pyroxenes. Meteoritics 18, 358.

Morrison, D., Harris, A. W., Sommer, G., Chapman, C. R., Carusi, A. 2002. Dealing with the Impact Hazard. In *Asteroids III* (Eds. W.F. Bottke, A. Cellino, P. Paolicchi, and R.P. Binzel), Univ. of Arizona Press, Tucson, 739-754.

Mothé-Diniz, T., Carvano, J. M. Á., Lazzaro, D. 2003. Distribution of taxonomic classes in the main belt of asteroids. Icarus 162, 10-21.

Nagasawa, M., Tanaka, H., Ida, S. 2000. Orbital Evolution of Asteroids during Depletion of the Solar Nebula. Astronomical Journal 119, 1480-1497.

Nagasawa, M., Ida, S., Tanaka, H. 2002. Excitation of Orbital Inclinations of Asteroids during Depletion of a Protoplanetary Disk: Dependence on the Disk Configuration. Icarus 159, 322-327.

Nesvorný, D., A. Morbidelli, D. Vokrouhlický, W. F. Bottke, and M. Brož 2002. The Flora Family: A Case of the Dynamically Dispersed Collisional Swarm? Icarus 157, 155-172.

Nesvorný, D., W. F. Bottke, L. Dones, and H. F. Levison 2002. The recent breakup of an asteroid in the main-belt region. Nature 417, 720-771.

Nesvorný, D., Bottke, W. F., Levison, H. F., Dones, L. 2003. Recent Origin of the Solar System Dust Bands. Astrophysical Journal 591, 486-497.

Nesvorný, D., Bottke, W. F. 2004a. Detection of the Yarkovsky effect for main-belt asteroids. Icarus 170, 324-342.

Nesvorný, D., Jedicke, R., Whiteley, R.J., and Ivezić, Ž. 2004. Evidence for asteroid space weathering from the Sloan Digital Sky Survey Icarus, in press.

Neukum, G. and B. A. Ivanov 1994. Crater Size Distributions and Impact Probabilities on Earth from Lunar, Terrestrial-planet, and Asteroid Cratering Data. In Hazards Due to Comets and Asteroids (Eds. T. Gehrels, M. S. Matthews) Univ. Arizona Press, Tucson, 359-416.

O'Brien, D. P. and R. Greenberg 2003. Steady-state size distributions for collisional populations:analytical solution with size-dependent strength. Icarus 164, 334-345.

O'Brien, D. P. and R. Greenberg 2005. The collisional and dynamical evolution of the main belt and NEA size distributions. Icarus, in press.

Opik, E. J. 1951. Collision probability with the planets and the distribution of planetary matter. Proc. R. Irish Acad. 54, 165-199.

Petit, J., Morbidelli, A., Valsecchi, G. B. 1999. Large Scattered Planetesimals and the Excitation of the Small Body Belts. Icarus 141, 367-387.

Petit, J., A. Morbidelli, and J. Chambers 2001. The Primordial Excitation and Clearing of the Asteroid Belt. Icarus 153, 338-347.

Petit, J.-M., J. Chambers, F. Franklin, and M. Nagazawa. 2002. Primoridal Excitation and Depletion of the Main Belt. In *Asteroids III* (Eds. W.F. Bottke, A. Cellino, P. Paolicchi, and R.P. Binzel), Univ. of Arizona Press, Tucson, 711-723.

Podolak, M. 2003. The contribution of small grains to the opacity of protoplanetary atmospheres. Icarus 165, 428-437.

Press, W. H., B. P. Flannery, S. A. Teukolsky and W. T. Vetterling 1989. Numerical recipes in Fortran. The art of scientific computing. Cambridge: University Press, 1989

Pollack, J. B., O. Hubickyj, P. Bodenheimer, J. J. Lissauer, M. Podolak, and Y. Greenzweig 1996. Formation of the Giant Planets by Concurrent Accretion of Solids and Gas. Icarus 124, 62-85.

Rabinowitz, D. L. E. Helin, K. Lawrence, and S. Pravdo. 2000. A Reduced Estimate of the Number of Kilometre-Sized Near-Earth Asteroids. Nature 403, 165-166

Richardson, J. E., Melosh, H. J., Greenberg, R. 2004. Impact-Induced Seismic Activity on Asteroid 433 Eros: A Surface Modification Process. Science 306, 1526-1529.

Rubincam, D. P. 2000. Radiative Spin-up and Spin-down of Small Asteroids. Icarus 148, 2-11.

Ryder, G., Koeberl, C., Mojzsis, S. J. 2000. Heavy Bombardment on the Earth at $\sim$ 3.85 Ga: The Search for Petrographic and Geochemical Evidence. In *Origin of the Earth and the Moon* (Eds, R. Canup and K. Righter) Univ. of Arizona Press, Tucson., 475-492.

Safronov, V. S. (1969) *Evolution of Protoplanetary Cloud and Formation of the Earth and Planets* Nauka, Moscow.

Schmidt, R. M., Housen, K. R. 1987. Some recent advances in the scaling of impact and explosion cratering. International Journal of Impact Engineering 5, 543-560.

Shoemaker, E.M., 1965. Preliminary analysis of the fine structure of the lunar surface in Mare Cognitum, in JPL Technical Report No. 32-700, pp. 75-134, and in *The Nature of the Lunar Surface* (Eds, W. N. Press et al.), 2, pp. 23-77, John Hopkins Press, Baltimore.

Shoemaker, E. M., and C. S. Shoemaker. 1996. The Proterozoic impact record in Australia. AGSO Journal of Australian Geology and Geophysics 16, 379-398.

Shoemaker, E. M. 1998. Long term variations in the impact cratering rate on Earth. In Meteorites: Flux with Time and Impact Effects, M. Grady, R. Hutchison R., G. J. H. McCall, and D. A. Rothery, Eds. Geological Society, London, Special Publications 140, 7-10.

Scott, E. R. D. 2002. Meteorite Evidence for the Accretion and Collisional Evolution of Asteroids. In *Asteroids III* (Eds. W.F. Bottke, A. Cellino, P. Paolicchi, and R.P. Binzel), Univ. of Arizona Press, Tucson, 697-709.

Scott, E. R. D., Haack, H., Love, S. G. 2001. Formation of mesosiderites by fragmentation and reaccretion of a large differentiated asteroid. Meteoritics and Planetary Science 36, 869-891.

Scott, E. R. D. 2003. Metallographic Cooling Rates of H Chondrites and the Structure of Their Parent Asteroid. Meteoritics and Planetary Science, vol. 38, Supplement, abstract no.5293 38, 5293.

Shukolyukov, A., Lugmair, G. W. 2002. Chronology of Asteroid Accretion and Differentiation. In *Asteroids III* (Eds. W.F. Bottke, A. Cellino, P. Paolicchi, and R.P. Binzel), Univ. of Arizona Press, Tucson, 687-695.

Slivan, S. M. 2002. Spin vector alignment of Koronis family asteroids. Nature 419, 49-51.

Slivan, S. M., Binzel, R. P., Crespo da Silva, L. D., Kaasalainen, M., Lyndaker, M. M., Krčo, M. 2003. Spin vectors in the Koronis family: comprehensive results from two independent analyses of 213 rotation lightcurves. Icarus 162, 285-30

Standish, E. M. 2001. JPL Interoffice Memorandum 312.F-01-006, April 11, 2001.

Stokes, G. H., D.K. Yeomans, W.F. Bottke, S.R. Chesley, J.B. Evans, R.E. Gold, A.W. Harris, D. Jewitt, T.S. Kelso, R.S. McMillan, T.B. Spahr, and S.P. Worden, *Report of the Near-Earth Object Science Definition Team: A Study to Determine the Feasibility of Extending the Search for Near-Earth Objects to Smaller Limiting Diameters*. NASA-OSS-Solar System Exploration Division, 2003.

Stuart, J. S. 2001. A Near-Earth Asteroid Population Estimate from the LINEAR Survey. Science 294, 1691-1693.

Stuart, J. S., Binzel, R. P. 2004. Bias-corrected population, size distribution, and impact hazard for the near-Earth objects. Icarus 170, 295-311.

Tanga, P., A. Cellino, P. Michel, V. Zappalà, P. Paolicchi and A. Dell'Oro 1999. On the size distribution of asteroid families: The Role of Geometry. Icarus 141, 65-78

Tedesco, E. F., Desert, F. 2002. The Infrared Space Observatory Deep Asteroid Search. Astronomical Journal 123, 2070-2082.

Tera, F., Papanastassiou, D. A., Wasserburg, G. J. 1974. Isotopic evidence for a terminal lunar cataclysm. Earth and Planetary Science Letters 22, 1-21.

Thomas, P. C., R. P. Binzel, M. J. Gaffey, A. D. Storrs, E. N. Wells, and B. H. Zellner 1997. Impact excavation on asteroid 4 Vesta: Hubble Space Telescope results. Science 277, 1492-1495.

Thommes, E. W., Duncan, M. J., Levison, H. F. 1999. The formation of Uranus and Neptune in the Jupiter-Saturn region of the Solar System. Nature 402, 635-638.

Thommes, E. W., Duncan, M. J., Levison, H. F. 2002. The Formation of Uranus and Neptune among Jupiter and Saturn. Astronomical Journal 123, 2862-2883.

Torigoye-Kita, N., Tatsumoto, M., Meeker, G. P., Yanai, K. 1995. The 4.56 Ga U—Pb age of the MET 780058 ureilite. Geochimica et Cosmochimica Acta 59, 2319-2329.

Trieloff, M., Jessberger, E. K., Herrwerth, I., Hopp, J., Fiéni, C., Ghélis, M., Bourot-Denise, M., Pellas, P. 2003. Structure and thermal history of the H-chondrite parent asteroid revealed by thermochronometry. Nature 422, 502-506.

Vedder, J. D. 1998. Main Belt Asteroid Collision Probabilities and Impact Velocities. Icarus 131, 283-290.

Viateau, B. 2000. Mass and density of asteroids (16) Psyche and (121) Hermione. Astronomy and Astrophysics 354, 725-731.

Vokrouhlický, D., Farinella, P. 2000. Efficient delivery of meteorites to the Earth from a wide range of asteroid parent bodies. Nature 407, 606-608.

Vokrouhlický, D. and D. Čapek 2002. YORP-Induced Long-Term Evolution of the Spin State of Small Asteroids and Meteoroids: Rubincam's Approximation. Icarus 159, 449-467.

Vokrouhlický, D., Nesvorný, D., Bottke, W. F. 2003. The vector alignments of asteroid spins by thermal torques. Nature 425, 147-151.

Ward, W. R. 1979. Present obliquity oscillations of Mars - Fourth-order accuracy in orbital E and I. Journal of Geophysical Research 84, 237-241.

Ward, W. R. 1981. Solar nebula dispersal and the stability of the planetary system. I - Scanning secular resonance theory. Icarus 47, 234-264.

Wasson, J. T., Wetherill, G. W. 1979. Dynamical chemical and isotopic evidence regarding the formation locations of asteroids and meteorites. In *Asteroids* (Ed. T. Gehrels) Univ. of Arizona Press, Tucson, 926-974.

Weidenschilling, S. J. 1977. The distribution of mass in the planetary system and solar nebula. Astrophysics and Space Science 51, 153-158.

Weidenschilling, S. J., D. Spaute, D. R. Davis, F. Marzari, and K. Ohtsuki 1997. Accretional Evolution of a Planetesimal Swarm. Icarus 128, 429-455.

Werner, S. C., Harris, A. W., Neukum, G., Ivanov, B. A. 2002. NOTE: The Near-Earth Asteroid Size-Frequency Distribution: A Snapshot of the Lunar Impactor Size-Frequency Distribution. Icarus 156, 287-290.

Wetherill, G. W. 1967. Collisions in the asteroid belt. Journal of Geophysical Research 72, 2429-2444.

Wetherill, G. W. and J. G. Williams 1979. Origin of differentiated meteorites. In: Origin and Distribution of the Elements. Volume 34. Proceedings of the Second Symposium, Paris, France, May 10-13, 1977. (A79-44751 19-91) London, Pergamon Press, Ltd.

Wetherill, G. W. 1989. Origin of the asteroid belt. In *Asteroids II* (Eds. R.P. Binzel, T. Gerhels, and M. S. Matthews), University of Arizona Press, 661-680.

Wetherill, G. W. 1992. An alternative model for the formation of the asteroids. Icarus 100, 307-325.

Wetherill, G. W. and G. R. Stewart 1989. Accumulation of a swarm of small planetesimals. Icarus 77, 330-357.

Williams, D. R. and G. W. Wetherill 1994. Size distribution of collisionally evolved asteroidal populations - Analytical solution for self-similar collision cascades. Icarus 107, 117.

Wilhelms, D. E., McCauley, J. F., Trask, N. J. 1987. The geologic history of the moon. Washington : U.S. Geological Survey. Denver, CO (Federal Center, Box 25425, Denver 80225)

Wilson, L., Keil, K. 1991. Consequences of explosive eruptions on small solar system bodies - The case of the missing basalts on the aubrite parent body. Earth and Planetary Science Letters 104, 505-512.

Wisdom, J. 1983. Chaotic behavior and the origin of the 3/1 Kirkwood gap. Icarus 56, 51-74.

Wuchterl, G., Guillot, T., Lissauer, J. J. 2000. Giant Planet Formation. In *Protostars and Planets IV* (Eds. V. Mannings, A. Boss, S. Russell), Univ. of Arizona Press, Tucson, 1081-1109.

Xu, S., Binzel, R. P., Burbine, T. H., Bus, S. J. 1995. Small main-belt asteroid spectroscopic survey: Initial results. Icarus 115, 1-35.

Yoshida, F., Nakamura, T. 2004. Basic nature of sub-km main-belt asteroids: their size and spatial distributions. Advances in Space Research 33, 1543-1547.

Zappalà, V., Cellino, A., dell'Oro, A., Paolicchi, P. 2002. Physical and Dynamical Properties of Asteroid Families. In *Asteroids III* (Eds. W.F. Bottke, A. Cellino, P. Paolicchi, and R.P. Binzel), Univ. of Arizona Press, Tucson, 619-631.

Table Captions

Table 1. Best fit results for the 550 CoDDEM runs from Fig. 12. Each run consists of 100 trial cases, with the Q_D^* function set to #10 (Fig. 5) and the initial size distribution set to $D_x = 110$ km (Fig. 9). Column 1 is the formation time of Jupiter ($t_{\rm Jup}$) in My. Column 2 is f, the initial size of $N_{\rm dep}$. We define $f = 1$ to be the amount of mass in the observed main belt (i.e., $5 \times 10^{-4} M_\oplus$). Column 3 is the number of times out of 100 trial cases that our metrics for success were met (i.e., $\psi^2_{\rm SFD} < 20$ and $\chi^2_{\rm FAM}$ exceeds a probability of 5%). All runs with values larger than 40 are reported in the table. Column 4 is the median value of $\psi^2_{\rm SFD}$ for the successful runs from Column 3. A line fit to these points in this table yields $f = 186$ My $- 8.2 t_{\rm Jup}$.
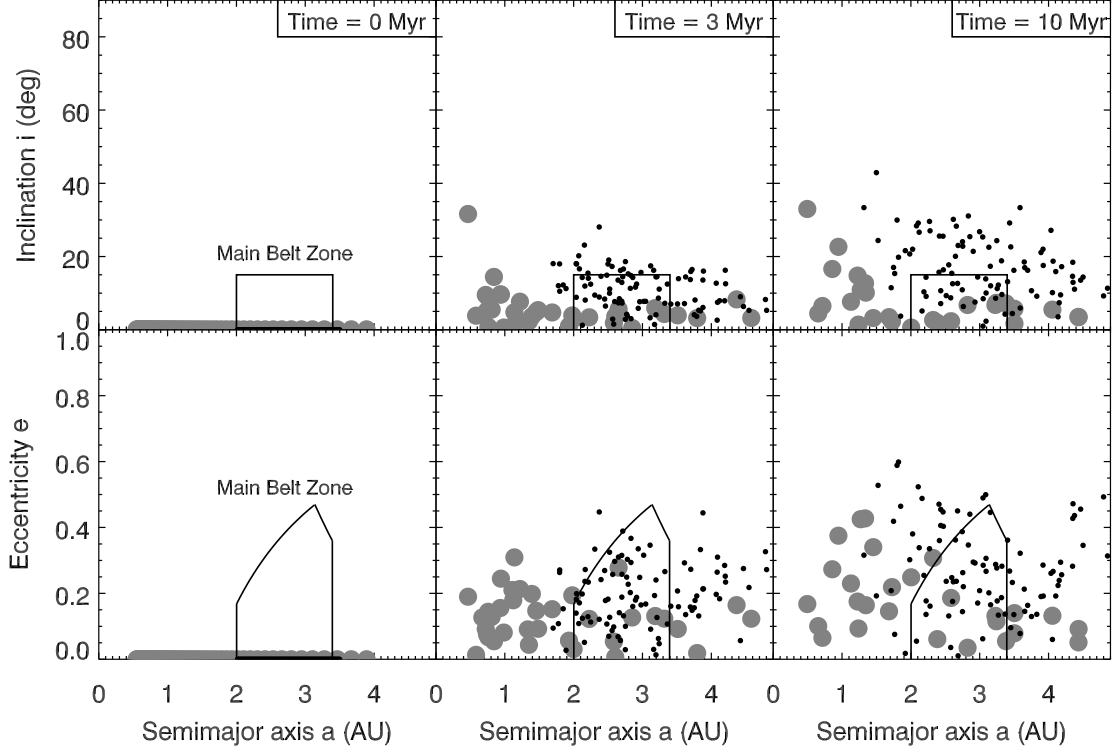
Fig. 1.— Three snapshots from a representative run in Petit *et al.* (2001), where the dynamical evolution of test bodies and planetary embryos were tracked for 10 My prior to the formation of Jupiter (Phase 1; see Sec. 2.2.1). The first timestep, $t = 0$ My, shows the initial conditions. The large gray dots represent 56 moon- to Mars-sized embryos started on circular, slightly inclined orbits ($i = 0.1°$) between 0.5 and 4 AU. The masses of the individual embryos were increased from the inner (1/60 Earth mass) to the outer edge (1/3 Earth mass) of the disk according to $\propto a^3 \sigma^{-3/2}$, where σ is the surface density of the protoplanetary disk. Their total mass was set to $5M_\oplus$. The smaller black dots represent 100 test bodies stared on circular, zero-inclination orbits between $2.0 < a < 3.5$ AU. The approximate orbital properties of the current main belt (i.e., the main belt zone) are shown as solid black lines. As time evolves, we see the embryos increasingly excite the test bodes and one another. After $t = 10$ My, some particles have reached $a \sim 1$ and 5 AU, $e \sim 0.6$, and $i \sim 40°$. Only 17 test bodies are left in the main belt zone at this time.
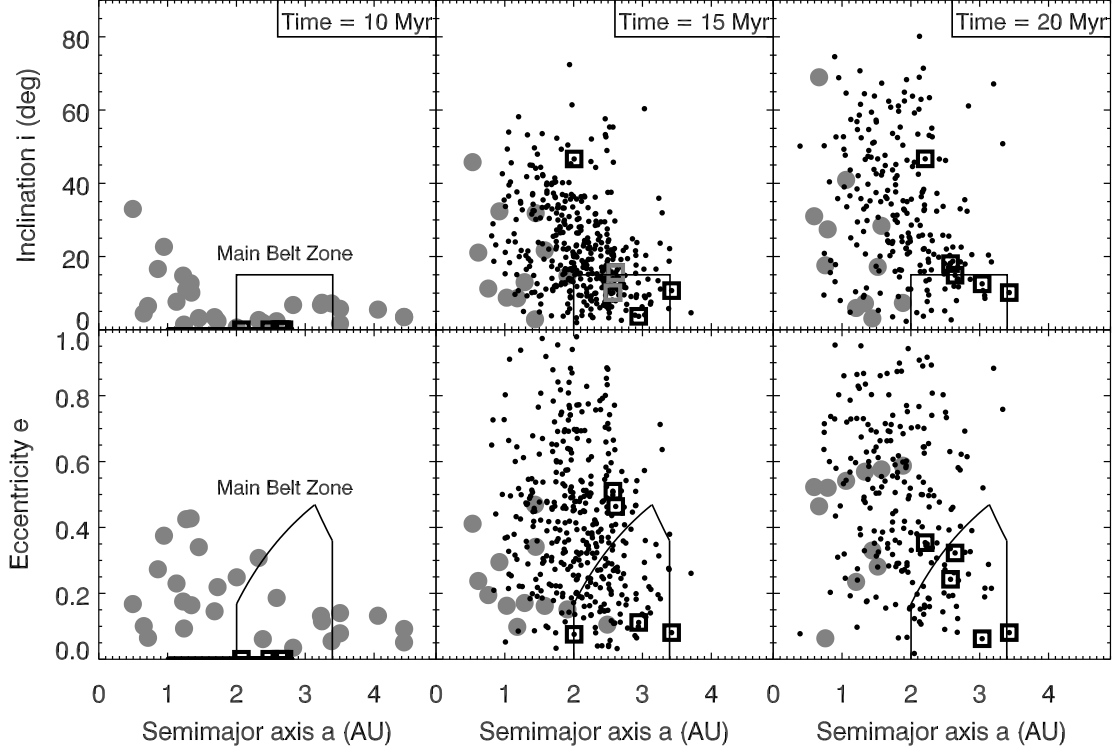
Fig. 2.— Three snapshots from a second representative run in Petit *et al.* (2001), where the dynamical evolution of test bodies and planetary embryos were tracked for more than 100 My just after the formation of Jupiter (Phase 2; see Sec. 2.2.2). The first timestep, $t = 10$ My, shows the initial conditions. The grey dots are planetary embryos whose orbital parameters were taken directly from the last frame of Fig. 1. The black dots represent two sets of test bodies: one set with 100 particles stared on circular, zero-inclination orbits between $1.0 < a < 2.0$ AU, and second set with 1000 particles stared on circular, zero-inclination orbits between $2.0 < a < 2.8$ AU. The black (or gray) squares are centered on the 5 test bodies that will ultimately be trapped in the main belt zone. At $t = 15$ My, nearly all of the test bodies have been pushed out of the main belt onto high e, i orbits. Perturbations from Jupiter have eliminated or forced the merger of many embryos. By $t = 20$ My, only a third of the original test bodies are still in the system. Some black square test bodies can be found outside the main belt zone during this time period.
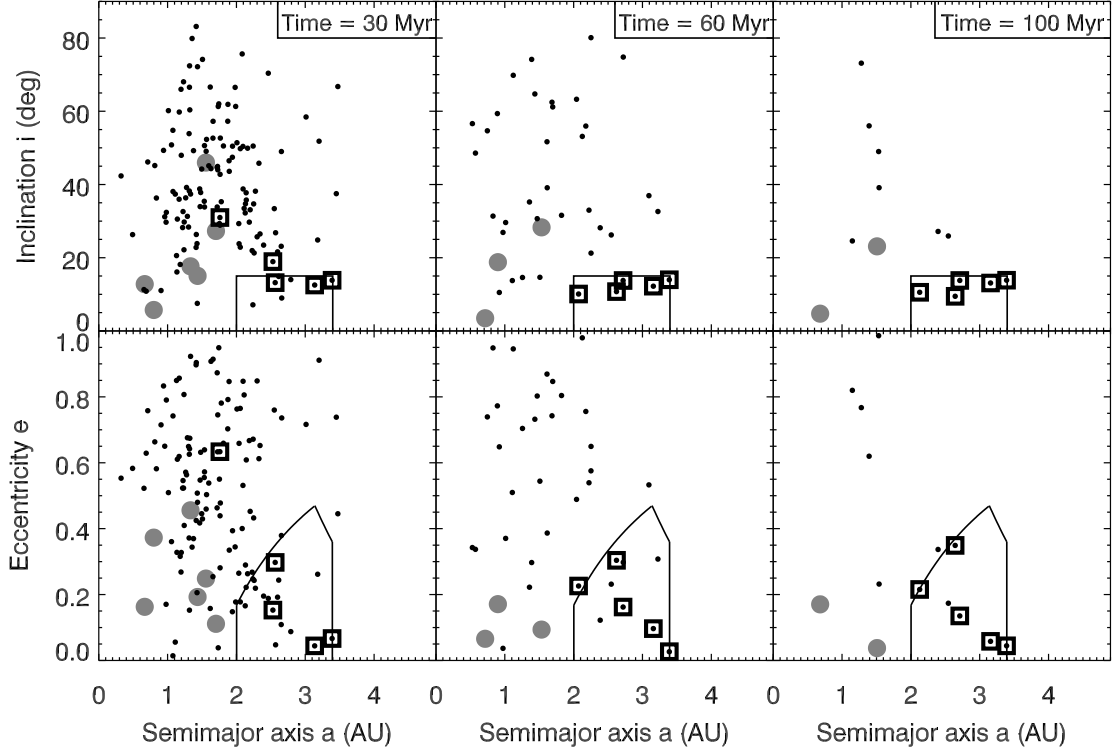
Fig. 3.— Three more snapshots from the run described in Fig. 2 (Phase 2; see Sec. 2.2.2). Here we see the embryos merging to form two terrestrial planets after 100 My, one with a mass of $1.3M_{\oplus}$ ($a = 0.68$ AU, $e = 0.15$, and $i = 5°$) and a second with $0.48M_{\oplus}$ ($a = 1.5$ AU, $e = 0.03$, and $i = 23°$). Neither planet crosses into the main belt region, though both are dynamically hot compared to our system of terrestrial planets. At $t = 60$ My, all 5 of the black square test bodies have become trapped in the main belt zone. Beyond these objects, only a few test bodies are left at $t = 100$ My. These survivors are cloned and tracked for an additional 400 My.
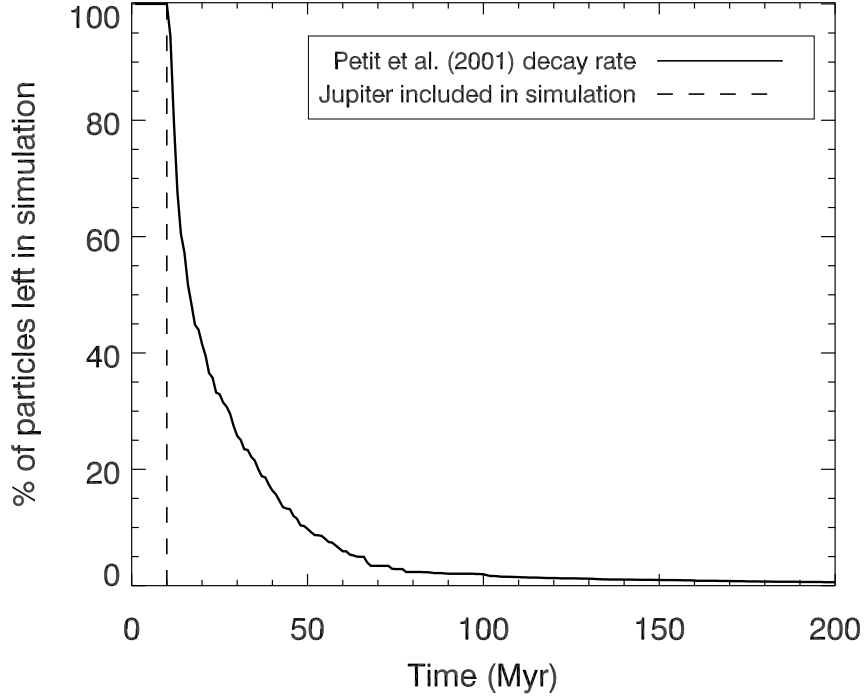
Fig. 4.— The decay rate of test bodies from the Petit *et al.* (2001) simulations shown in Figs. 2 and 3. We assume that few particles are lost in Phase 1 prior to the formation of Jupiter. Here Jupiter enters the system at $t_{\rm Jup} = 10$ My, though our CoDDEM runs (see Sec. 3) allow $t_{\rm Jup}$ to vary between 1-10 My. The decay rate was estimated by tracking the number of surviving test bodies over time. Particles are eliminated by striking a planetary embryo, the Sun, or being thrown out of the inner solar system via a close encounter with Jupiter. The decay rates of test bodies between $1.0 < a < 2.0$ AU (e.g., Fig. 2) were normalized in order to merge them with the number of particles used in the $2.0 < a < 2.8$ AU runs.
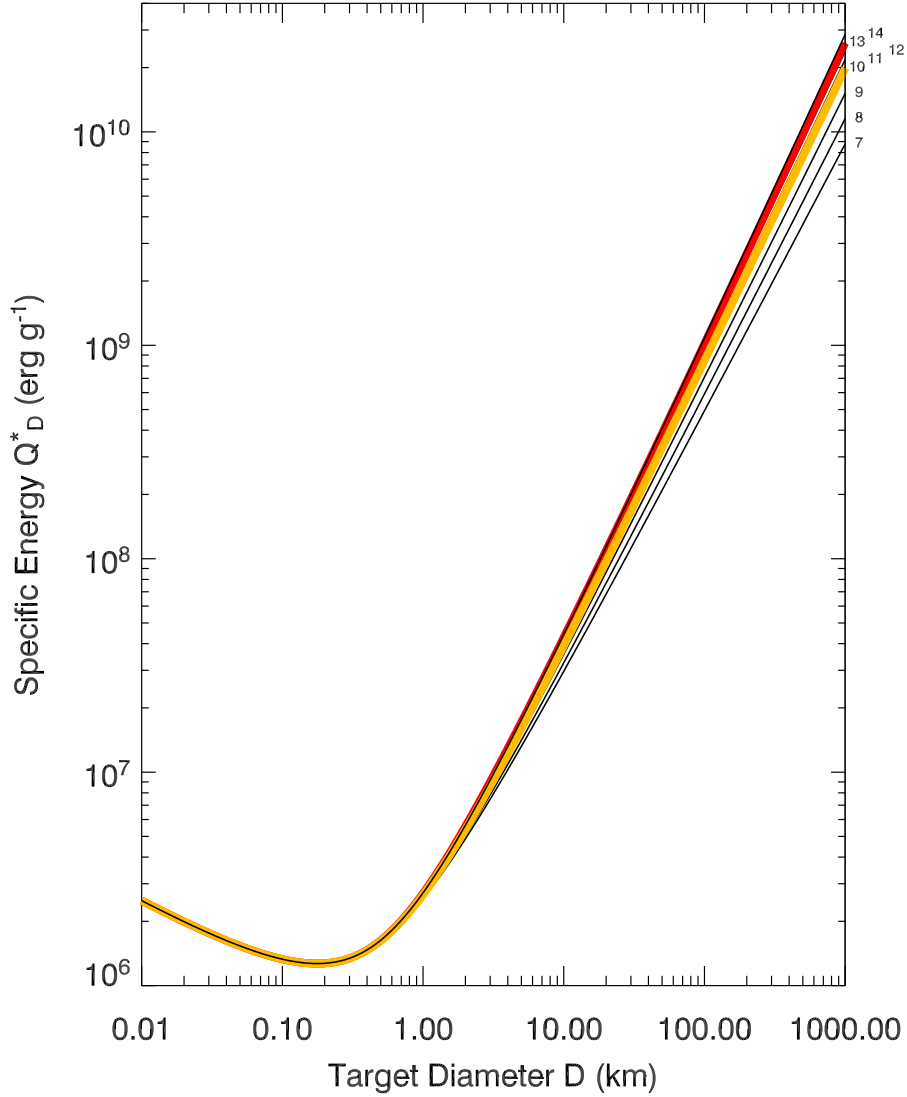
Fig. 5.— The critical impact specific energy, Q_D^*, is defined as the energy per unit target mass delivered by the projectile required for catastrophic disruption of the target (i.e., such that one-half the mass of the target body escapes). The Q_D^* functions used in CoDDEM were the best-fit cases defined by Bottke *et al.* (2004). Using their numbering scheme, we test their Q_D^* functions #7-#14. For reference, the Q_D^* function computed by Benz and Asphaug (1999) for projectiles striking undamaged basaltic target bodies at $V = 3$ km s^{-1} is #13 (red curve). The most successful Q_D^* function used in this paper is #10 (gold curve). All the functions pass through the normalization point $Q_D^* = 1.5 \times 10^7$ erg g^{-1} and $D = 8$ cm, a value determined using laboratory impact experiments (e.g., Durda *et al.* 1998).
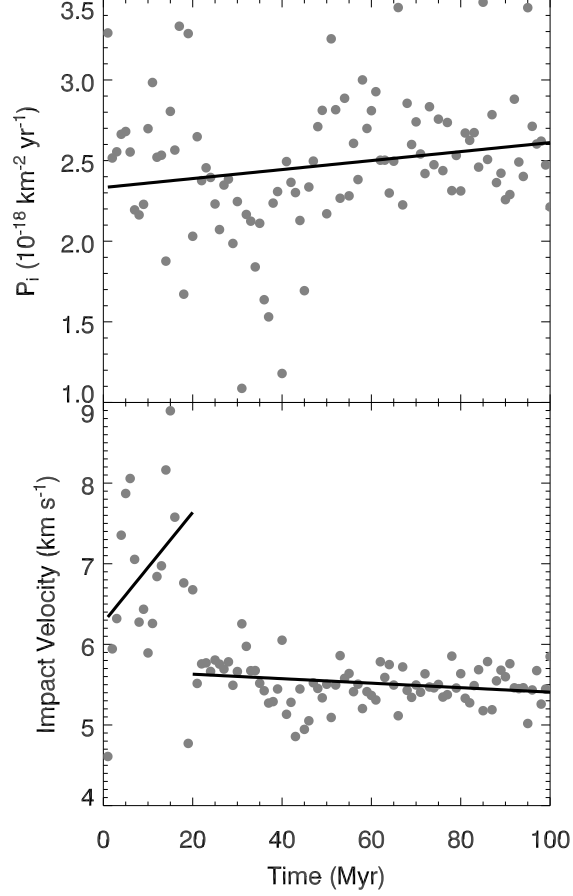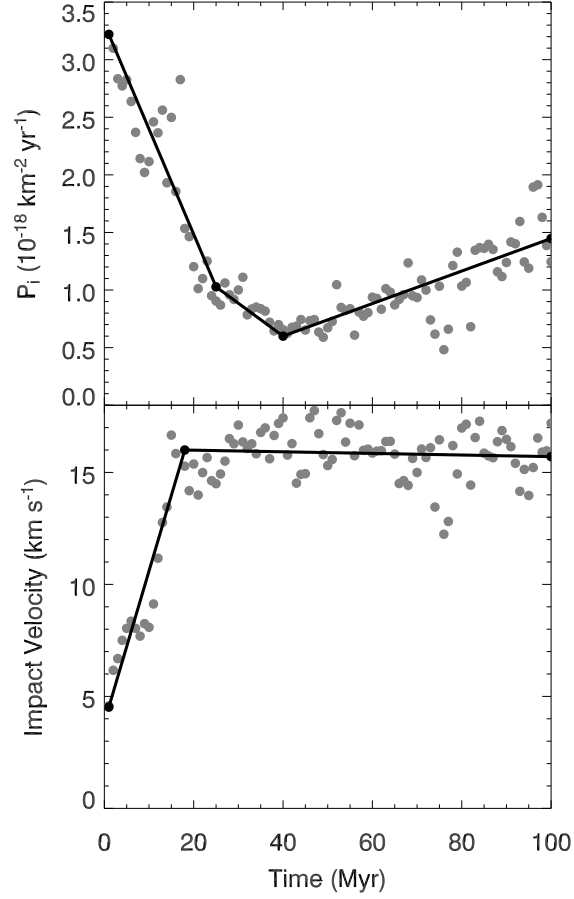
Fig. 6.— The intrinsic collision probabilities (P_i) and impact velocities (V_{imp}) for bodies in the remnant main belt population N_{rem} (i.e., the planetesimals remaining in the main belt zone) colliding amongst themselves. These values are computed using the (a, e, i) values of the test bodies shown in Figs. 1, 2 and 3. Details on our procedure are given in Sec. 3.2.2. The large impact velocities seen between $0 < t < 20$ My are produced by test bodies that temporarily escape the main belt zone only to return at a later time. The values of P_i and V_{imp} used in our code are represented by the solid line segments, which were computed using least squares fits to the plotted points.

Fig. 7.— The intrinsic collision probabilities (P_i) and impact velocities (V_{imp}) for bodies in the remnant main belt population (N_{rem}) colliding with bodies in the dynamically depleted population defined by N_{dep} (i.e., those bodies ejected from the main belt zone). Here the impact velocities are high because the portion of the N_{dep} population crossing the N_{rem} population has high e, i values.
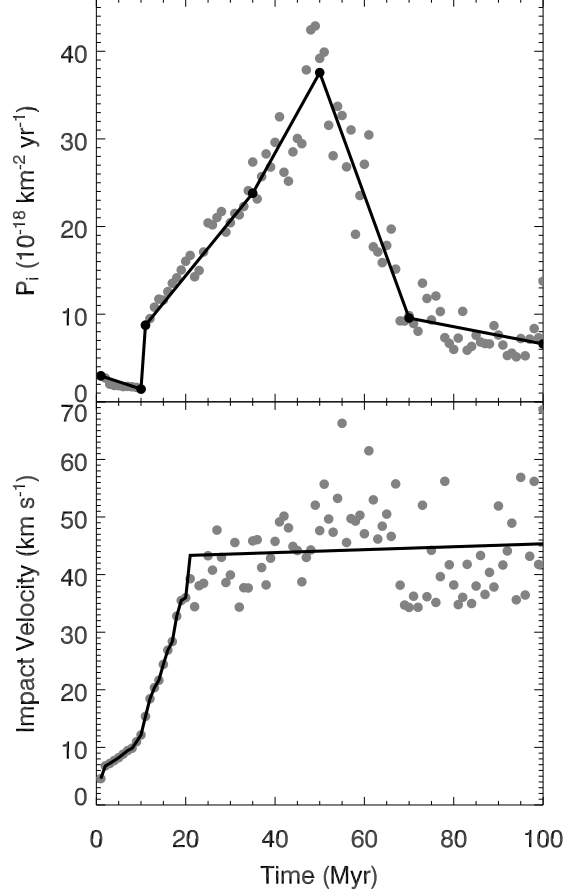
Fig. 8.— The intrinsic collision probabilities (P_i) and impact velocities (V_{imp}) for bodies in the dynamically depleted population (N_{dep}) colliding amongst themselves. The values of P_i and V_{imp} become extremely high over time because the bodies that survive the longest have low a and high e, i orbits.
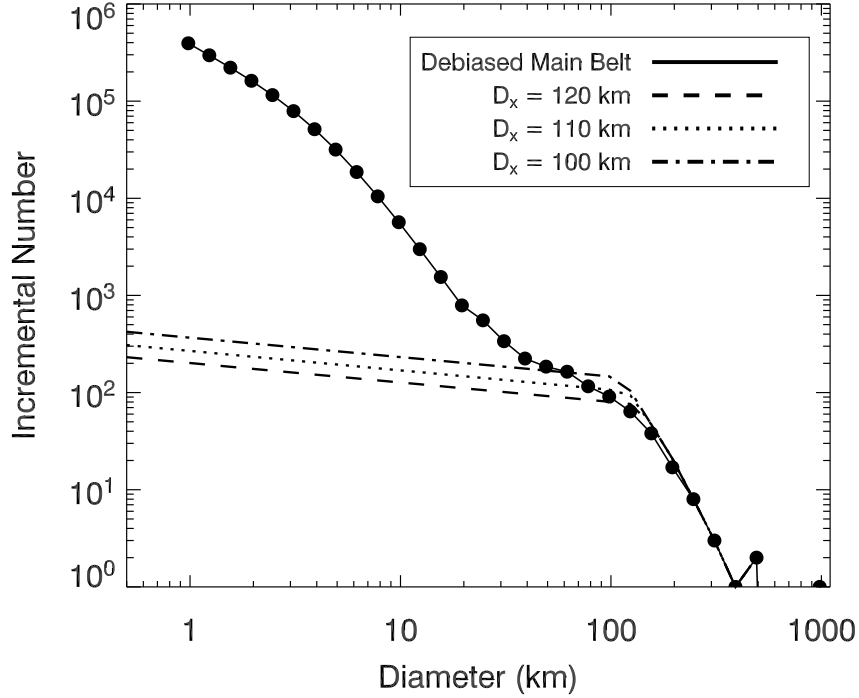
Fig. 9.— The initial main belt size distributions for $N_{\rm rem}$. We assumed the number of $D > 200$ km asteroids mimicked the observed main belt because very few of these object ever disrupt. For $D < 200$ km objects, we used a differential power law index of -4.5 until an inflection point D_x was reached ($D_x = 100$, 110, and 120 km). For $D < D_x$, the size distribution was given a shallow slope (-1.2) (for additional discussion, see Bottke *et al.* 2005). Also plotted is the main belt size frequency distribution, which was computed from a parametric representation of the absolute magnitude H distribution (Jedicke *et al.* 2002). The H bins were transformed into D bins using the geometric albedo $p_v = 0.092$. The dots show the position of each incremental bin. The main belt size-frequency distribution is wavy, with "bumps" near $D \sim 100$ km and $D \sim 3\text{-}4$ km. Using this population, the cumulative number of $D > 1, 50$, and 100 km asteroids is 1.36×10^6, 680 and 220, respectively.
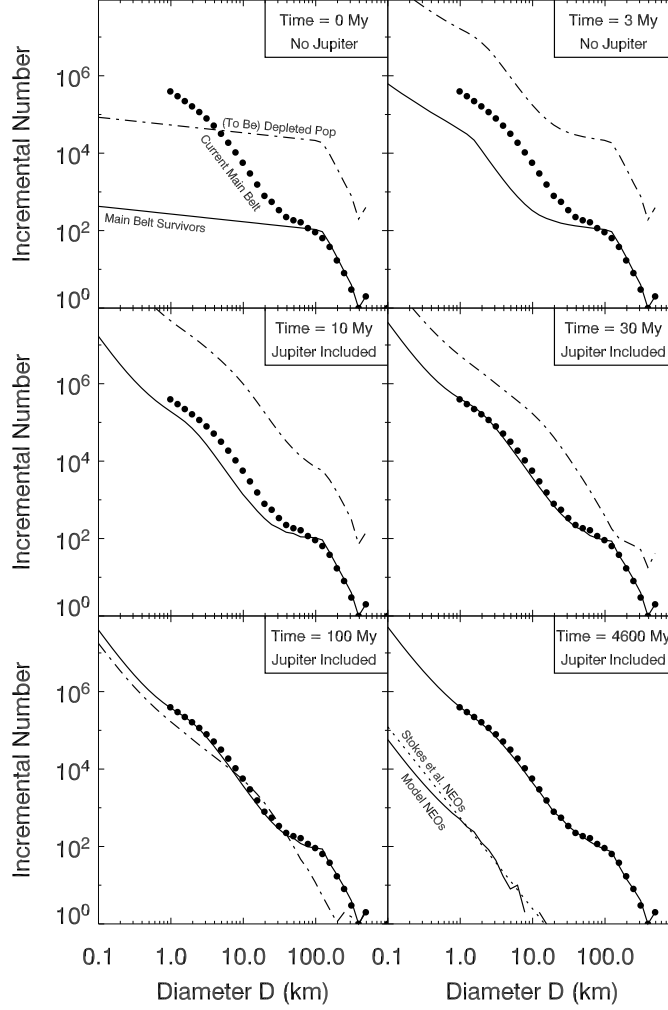
Fig. 10.— Six snapshots from a CoDDEM trial case where we tracked the collisional evolution of the main belt size distribution for 4.6 Gy. The initial populations use $D_x = 110$ km (Fig. 9) and $N_{\rm dep} = 200\,N_{\rm rem}$ (i.e., $f = 200$). The $Q_{\rm D}^*$ function was set to #13 (Fig. 5). We assume Jupiter enters the system at $t_{\rm Jup} = 4$ My. The $N_{\rm rem}$ population is shown as a solid line, while $N_{\rm dep}$ is given as a dot-dash line. Recall that the total population $N = N_{\rm rem} + N_{\rm dep}$; they are only separated for computational convenience. The dots represent the size distribution of the observed main belt. The bump observed in most frames near $D \sim 2$- 4 km is driven by the transition at $D \sim 0.2$ km between the strength and gravity-scaling regimes in $Q_{\rm D}^*$ (Fig. 5). The dynamical depletion of $N_{\rm dep}$ can be seen in timesteps $t = 10$-100 My. Our best-fit case is shown at $t = 4.6$ Gy. The $\psi_{\rm SFD}^2$ values for timesteps $t = 0, 3, 10, 30, 100$, and 4600 My are 372, 335, 237, 23.5, 24.4, and 9.3, respectively. Recall that our criteria for a nominal match between model and data is $\psi_{\rm SFD}^2 < 20$. The $t = 4.6$ Gy timestep also shows the NEO population produced by our model. For reference, we also plot the population estimates of Stokes *et al.* (2003). See Sec. 5.4 for details.
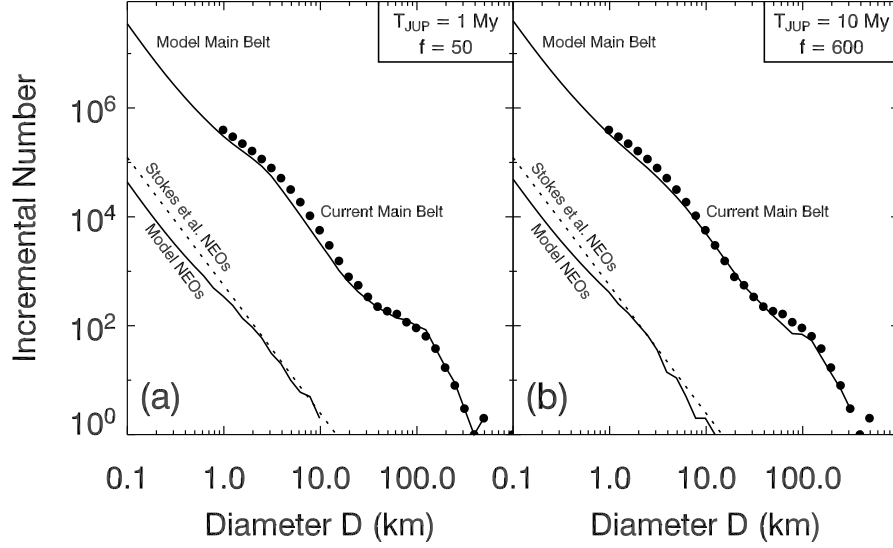
Fig. 11.— Two representative trial cases that did not meet our success metrics at $t = 4.6$ Gy. Both used $D_x = 110$ km (Fig. 9) and Q_D^* function #13 (Fig. 5). For (a), $N_{\text{dep}} = 50 N_{\text{rem}}$ (i.e., $f = 50$) and $t_{\text{Jup}} = 1$ My. Here insufficient comminution takes place to match the observed main belt. For (b), $f = 600$ and $t_{\text{Jup}} = 10$ My. In this case, collisions between N_{rem} and N_{dep} decimate the N_{rem} population over the $20 < D < 100$ km size range, such that the model population cannot reproduce the observed main belt. This model also produces a poor fit to the number of asteroid families produced by $D > 100$ km breakups over the last 3.5 Gy.
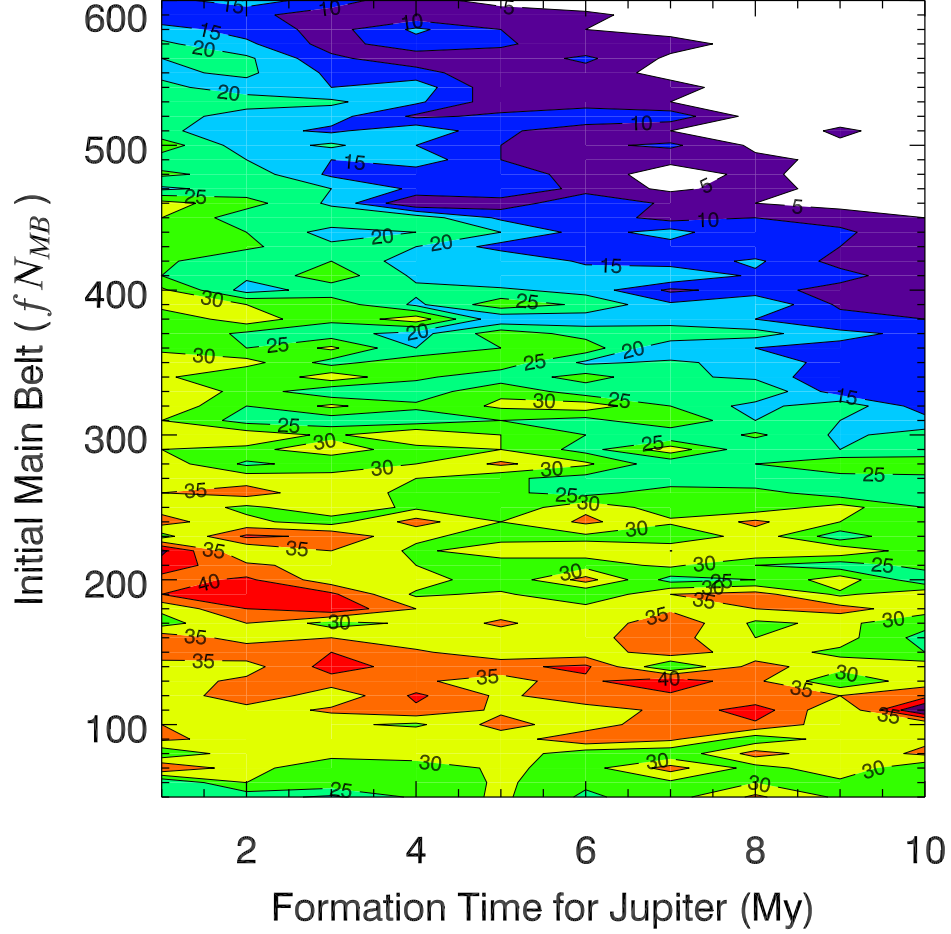
Fig. 12.— Contour plot showing CoDDEM results for $D_x = 110$ km (Fig. 9) and Q_D^* function #10 (Fig. 5). The x-axis shows the formation time of Jupiter (t_{Jup}), measured from the onset of fragmentation in the primordial main belt population. The y-axis shows the initial size of the primordial main belt population f, in units of the current main belt population ($N_{MB} \sim 5 \times 10^{-4} M_\oplus$). We set our input parameters to $t_{Jup} = 1$-10 My (incremented by 1 My) and $f = 50$-600 (incremented by 10). For each (t_{Jup}, f) combination, we performed 100 trials using our code CoDDEM. We define this as a "run". Thus, the contour plot represents the results of 550 runs or 55,000 distinct trial cases. The contours show the number of trial cases in each run that provide an acceptable match to the observed asteroid families (using χ_{FAM}^2) and the shape of the observed main belt size distribution (using ψ_{SFD}^2). See text for details. The peak values are reported in Table 1. We see the best fit cases adhere to an envelope of values with $f \sim 200$ for low t_{Jup} values and $f \sim 100$ for high t_{Jup} values.
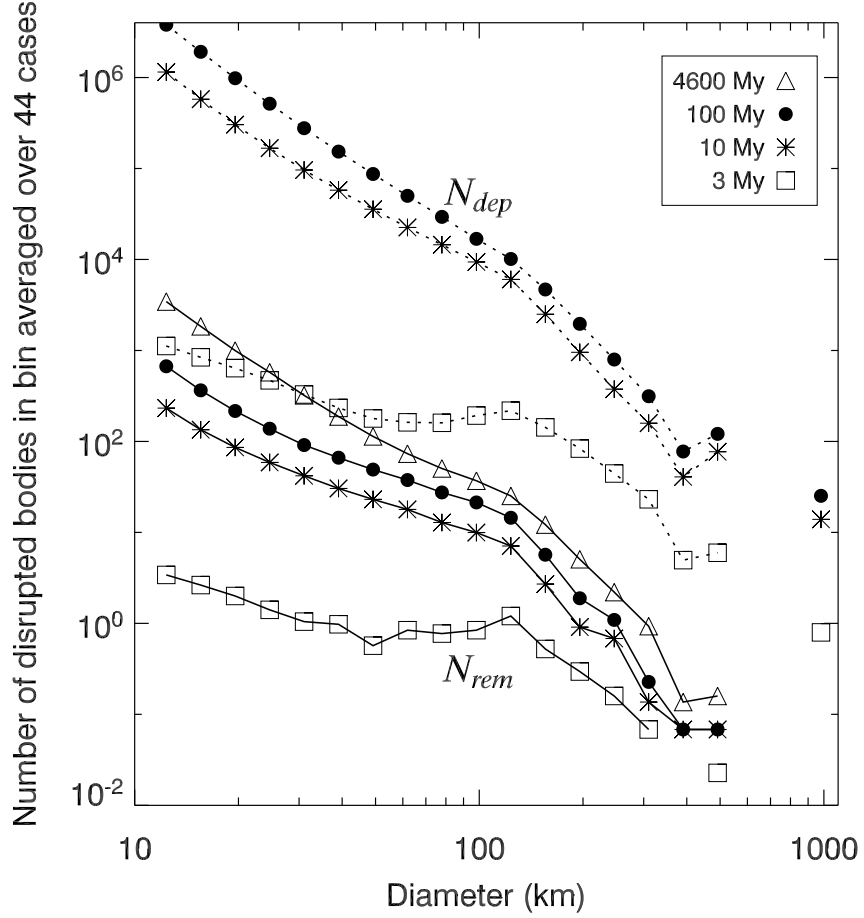
Fig. 13.— The average number of catastrophically disrupted bodies in each diameter bin for the Table 1 run where $t_{\mathrm{Jup}} = 3$ My, $f = 180$, $D_x = 110$ km, and Q_{D}^* function #10. These values were obtained by averaging results from the 44 trial cases where our success metrics were met. The colors describe these values at 3, 10, 100, and 4600 My. The points connected by the dotted lines represent disrupted asteroids from N_{dep}, while those connected by the solid line are from N_{rem}. According to Fig. 4, nearly all of N_{dep} has been dynamically eliminated after 100 My.
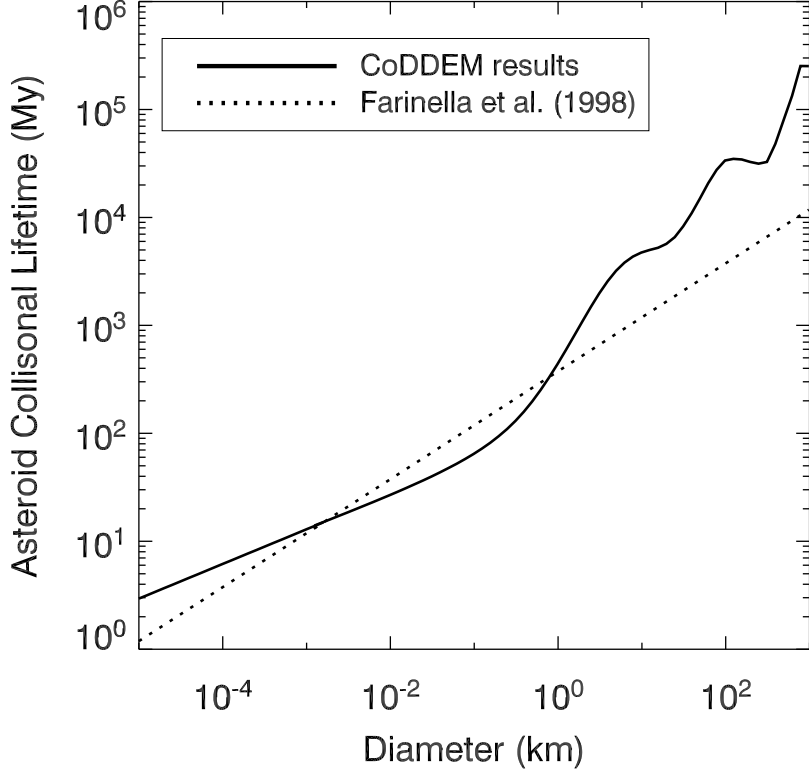
Fig. 14.— The collisional lifetime (τ) of main belt asteroids in CoDDEM. For comparison, we also plot $\tau = 16.8\,\mathrm{My} \times \sqrt{R(\mathrm{m})}$, a function derived by Farinella *et al.* (1998). For cm-sized objects, we obtained $\tau \sim 3$ My, consistent with estimated fireball lifetimes (Morbidelli and Gladman 1998). For meter-sized objects, we estimate $\tau \sim 14$ My. These values match the cosmic ray exposure ages of stony meteorites (e.g., Eugster 2003). For $1 \lesssim D \lesssim 100$ km asteroids, our values differ from Farinella *et al.* (1998); as described in the text, we believe our values are consistent with observations and modeling work of Koronis-family asteroids (Vokrouhlický *et al.* 2003). Finally, for $D > 100$ km asteroids, we find extremely long lifetimes, such that only ~ 4 of them (out of ~ 220) disrupt every Gy. This value provides a good match to the number of observed asteroid families produced by the breakup of such bodies over the last 3.5 Gy.
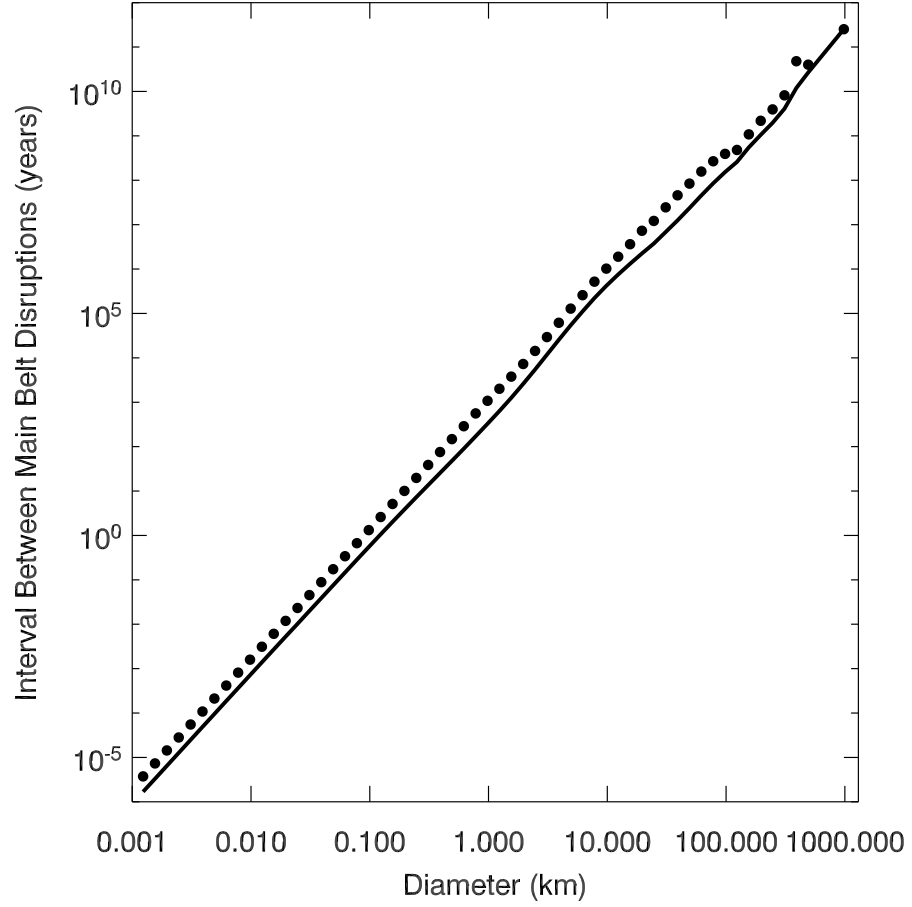
Fig. 15.— The interval between disruption events taking place across the main belt as a function of size. The black dots are the interval in each logarithmic size bin, while the solid line is the interval for asteroids larger than a given diameter.
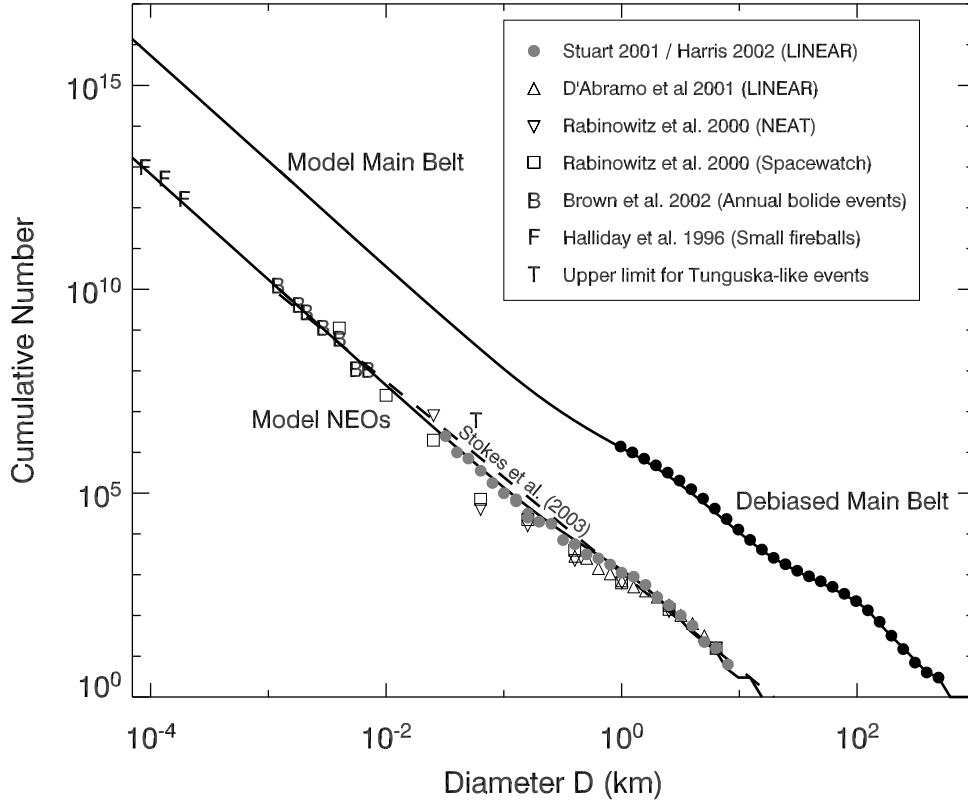
Fig. 16.— Our estimated values of the present-day main belt and NEO populations according to our CoDDEM model runs (solid lines). For reference, we plot our results against an estimate of the NEO population made by Stokes *et al.* (2003), who assumed the $D < 1$ km size distribution was a power-law extension of the $D > 1$ km size distribution. Our model main belt population provides a good match to the observed main belt (solid black dots). Most diameter $D \lesssim 100$ km bodies are fragments (or fragments of fragments) derived from a limited number of $D \gtrsim 100$ km breakups (Bottke *et al.* 2005). Our NEO model population is compared to estimates derived from telescopic sur;veys (Rabinowitz *et al.* 2000; D'Abramo *et al.* 2001; Stuart 2001; Harris 2002; Stuart and Binzel 2004), satellite detections of bolide detonations in Earth's atmosphere (Brown *et al.* 2002), and ground-based camera observations of fireballs (Halliday *et al.* 1996). For reference, we also include an upper limit estimate of 50 m NEOs based on the singular airblast explosion that occurred over Tunguska, Siberia in 1908 (e.g., Morrison *et al.* 2002; Stokes *et al.* 2003). The similarity between the shapes of the main belt and NEO populations is a byproduct of Yarkovsky thermal drag, which causes main belt asteroids with $D \lesssim 30$ km to drift into resonances that in turn deliver them to the NEO population.